

ESD-TDR-64-591

RETURN TO  
SCIENTIFIC & TECHNICAL INFORMATION DIVISION  
(ESTI), BUILDING 1211

COPY NR. \_\_\_\_\_ OF \_\_\_\_\_ COPIES

*ESRL*

ESTI PROCESSED

DDC TAB  PROJ OFFICER

ACCESSION MASTER FILE

\_\_\_\_\_

DATE \_\_\_\_\_

ESTI CONTROL NO. **AL 45438**

CY NR. 1 OF 1 CYS

# Technical Report

369

F. Belvin  
T. J. Goblick, Jr.

## Study of an Orbiting Dipole Belt Communication System

22 December 1964

Prepared under Electronic Systems Division Contract AF 19 (628)-500 by

# Lincoln Laboratory

MASSACHUSETTS INSTITUTE OF TECHNOLOGY

Lexington, Massachusetts



*A 00 413 583*



MASSACHUSETTS INSTITUTE OF TECHNOLOGY  
LINCOLN LABORATORY

STUDY OF AN ORBITING DIPOLE BELT  
COMMUNICATION SYSTEM

*F. BELVIN*  
*T. J. GOBLICK, JR.*

*Group 66*

TECHNICAL REPORT 369

22 DECEMBER 1964

## ABSTRACT

The design of communication systems utilizing orbiting dipole belts is complicated by the great amount of interaction among the various design parameters involved. This interaction makes difficult a general treatment of the design problem for such systems, necessitating the study of specific examples. This report studies in detail the simplest example of such a system in which a single equatorial dipole belt is used. An altitude of 8000 miles is used to provide satisfactory earth coverage. This altitude precludes the possibility of a limited orbital lifetime belt. An 800-kg payload of X-band, copper dipoles would provide modest data rates which should suffice for certain military needs. Insofar as a specific belt configuration and dipole design were chosen, the specific results of this work do not apply to dipole belt systems in general. However, the considerations that receive attention, and the approach used in dealing with them, can be used as a guide in the design of any dipole belt communication system.

Accepted for the Air Force  
Stanley J. Wisniewski  
Lt Colonel, USAF  
Chief, Lincoln Laboratory Office

## TABLE OF CONTENTS

Abstract	iii
I. Introduction	1
A. Military Requirements	2
B. System Design Problems	2
C. System Choice	3
D. Summary	5
II. Dipole Belt Physical Characteristics	7
A. General Behavior	7
B. Belt Formation	8
C. Belt Discription	9
D. Optieal Brightness	11
E. Collision Interference	15
III. Coverage	17
A. Belt Visibility	17
B. Belt Coverage	21
C. Network Organization	21
IV. Channel Characteristics	25
A. General	25
B. Received Power	30
C. Multipath Spread	33
D. Doppler Spread	33
E. Receiver Sensitivity	42
F. System Operating Margins	44
V. Communication Techniques	47
A. Introduction	47
B. M-ary Systems	51
C. Signal Design	53
VI. Communiciation Link Design	59
A. Graphical Determination of Modulation Parameters	59
B. Link Calculations	61

VII. Epilogue	65
A. Summary	65
B. Applicability of This Report	65
C. Caveat Emptor	66
Appendix A – Upper Bound on Binary Error Probability	67
Appendix B – $2r_e$ BeIt Parameters	71
I. Dipoles	71
II. Dispenser	71
III. Orbit	71
IV. Micrometeoroid Collision Models	72
Appendix C – Orbiting Dipoles as Puncture Hazard	73
I. Collision Rate	73
II. Collision Damage	74

# STUDY OF AN ORBITING DIPOLE BELT COMMUNICATION SYSTEM

## I. INTRODUCTION

At present, there is keen interest in world-wide communications networks – both on the part of commercial enterprises and in government/military circles. This interest is generally focused on accomplishing such feats by either active or passive earth satellites. It is hard to say whether the interest in communications has spurred the development of communications satellites or that the reverse is true. Nevertheless, it is generally agreed that a communication satellite system is the best way to realize the world-wide communication network.

Several features of the satellite communication system business distinguish it from earlier communication system problems. First, satellite communication systems offer a disarming array of alternatives – each of which must be resolved by choice before one has even a paper design of a communication system to evaluate. Second, the costs, at least at present and in the foreseeable future, are very high, so that experiment is generally held to a minimum. Finally, there is the very definite probability that the hardware placed in orbit may cease functioning quite quickly, returning very little in service for a very large outlay of capital.

We will discuss only one of the many alternatives in satellite communication systems which is particularly well suited to a segment of government/military communication requirements. Project West Ford was intended to demonstrate, and indeed has demonstrated, the feasibility of using a belt of orbiting copper dipoles as a scattering medium for microwaves. An experimental dipole belt was successfully launched in May 1963 and a complete record of results of this experiment was published in an issue of the Proceedings of the IEEE which was devoted to the West Ford program.

Ever since an orbiting dipole belt was first proposed for communications by H. Meyer and W.E. Morrow, Jr.,<sup>1</sup> the concept has been opposed by some scientists who feared that cluttering a large volume of space around the earth might hamper future astronomical observations. This opposition is likely to be a potent factor in any consideration of orbiting dipoles for a practical communication system. It seems clear that the decision to launch dipole belts in the future will be made only at very high government levels.

The published reports concerning Project West Ford contain the theory of the dipole belt formation, results of measurements of belt physical characteristics and communication experiments, and a description of the equipment used in the experiment. The present report is intended to complement the Project West Ford reports in going one step beyond the experimental dipole belt. Based on the results of Project West Ford, we will examine the applicability of dipole belts to the problem of reliable world-wide communication systems. We will thus assume familiarity on the part of the serious reader with the published reports on Project West Ford.

A belt of orbiting dipoles has several fundamental advantages which make it attractive for certain types of government/military communication systems. The most outstanding of these advantages are:

- (a) Reliability of passive satellites,
- (b) A highly dispersed satellite system assuring invulnerability to both physical and electronic countermeasures,
- (c) Maximum ground coverage for any given number of orbits,
- (d) The ultimate in a multiple access system.

Further advantages which may be of lesser importance are:

- (a) A single high-altitude dipole belt (from a single launch) can provide quite adequate earth coverage;
- (b) Antenna aiming and tracking problems are minimal since individual satellites do not need to be followed.

The most significant disadvantages of such a communication system are:

- (a) Passive communication satellites provide low information capacity;
- (b) Closure time, the time to form a complete belt once the dipoles are dispensed, precludes use as an emergency system;
- (c) Opposition to launching future dipole belts because of possible interference with astronomical observations, which may deter the deployment of a dipole belt system.

#### A. MILITARY REQUIREMENTS

The large costs of space-communications systems make large communication capacity of prime importance in a commercial system in order to reduce the cost per unit of capacity. This consideration alone is enough to rule dipole belts out of commercial systems. The prime requirements of a military communication system may be classified into the following categories:

- (1) Information capacity,
- (2) Earth coverage,
- (3) Invulnerability to enemy countermeasures,
- (4) Cost to bring to operational status,
- (5) Expected communication lifetime,
- (6) Time to bring to operational status,
- (7) Use with small, mobile, or transportable ground terminals.

In the case of orbiting dipole belt systems, several side issues which must definitely be contended with are:

- (8) Orbital lifetime,
- (9) Optical brightness,
- (10) Collision hazard to spacecraft presented by the belt,
- (11) Radar reflectivity.

#### B. SYSTEM DESIGN PROBLEMS

It is not difficult to show that 800 kg of copper dipoles placed in a very tight belt<sup>†</sup> would support teletype communication with reasonably small terminal equipment. Questions about dipole belts for communication may all be directed at the formation and maintenance of a very tight belt. The design of the belt (dipoles, dispenser, and orbit) is the heart of the problem, which is, unfortunately, a difficult one. Essentially the only tool available to aid in designing

<sup>†</sup> The terminology "very tight belt" is meant to imply the ultimate in a tight belt, namely, all dipoles in precisely the same orbit and uniformly distributed around the orbit.

dipole belts is a digital computer simulation program which simulates the behavior of dipoles in orbit for long periods of time. Hence, design of dipole belts is largely a process of trial designs and computer simulation.

The actual physical parameters of a dipole belt communication system are many. We list below some of the major parameters.

- (1) Space Payload
  - Total weight of dipoles and dispenser
  - Dipole material
  - Dipole dimensions
  - Blackening of dipoles
- (2) Orbit Parameters
  - Number of belts
  - Altitude
  - Inclination
  - Eccentricity of each belt
- (3) Terminal Equipment
  - Operating frequency
  - Transmitter power
  - Antenna sizes
  - Receiver noise temperature
  - Modulation system parameters.

Unfortunately, there is no simple one-to-one relationship between the parameters and system requirements. If we were to list both the parameters and requirements side by side on the same sheet of paper, we could draw lines from each of the requirements to all the parameters that affect that requirement. After filling in such lines for every item in the list of requirements, we would find that almost every possible line would be drawn. This implies a strongly interacting design problem in which almost every parameter affects almost every one of the items in the list of requirements.

### C. SYSTEM CHOICE

The fundamental questions concerning a satellite communication system are: (1) can we communicate satisfactorily? and (2) do we have adequate coverage for a given network of stations? If either of these questions must be answered in the negative, we need not concern ourselves with any other system requirements. We already know how to calculate data rates for extremely tight dipole belts and we know that belts can give excellent coverage. Therefore, we can answer the two questions posed above by simply determining the payload weight and orbit parameters that can be provided by present day launch vehicles. This puts a rather tight bound on the main questions of information capacity and coverage.

The invulnerability to physical and electronic countermeasures is essentially the same for all dipole belts and therefore this item can be eliminated from the design problem. The next important question is that of cost - in money, time, launch vehicles, etc. Only when we have established the feasibility of an orbiting dipole belt system with respect to information capacity, coverage, and cost, will we need to concern ourselves with items (8), (9), (10), and (11) in the requirements list.

It is on the items of cost, time to operational status, and expected communication lifetime that we find a clear dichotomy in belt designs. This dichotomy is between limited-lifetime dipole belts and indefinite, possibly unlimited, orbital lifetime belts. A dipole payload may be designed and orbited to have the cumulative effect of solar radiation pressure perturb the belt orbit until it re-enters the earth's atmosphere, thereby removing the dipoles from orbit. The Project West Ford experimental dipole belt was designed to have a lifetime of from three to five years before solar radiation pressure swept the orbit into the atmosphere. Radar measurements confirm that the experimental belt is behaving as predicted.

The motivation for limited-lifetime belts stems from the strong objection by some astronomers to the placing of billions of small particles into a large volume of space. The limited-lifetime requirement places severe constraints on belt altitudes, inclinations and on dipole area-to-mass ratios. Low belt altitudes (less than 5000 miles) are necessary to sufficiently limit belt lifetime even with dipoles of large area-to-mass ratios ( $80$  to  $100 \text{ cm}^2/\text{gm}$ ). Practical limited-lifetime belts are characterized by an approximately linear decrease in perigee height with time and by a continually decreasing average dipole density as the belt disperses. Such belts have perigee heights which, already small to meet the limited-lifetime (resonance) requirements, decrease during the belt lifetime, thereby severely limiting the communication coverage. The continual density reduction and lowering of belt altitude combine to reduce the scattering cross section in orbit mutually visible to two sites to small values early in the belt's life. Therefore, a system based on limited-lifetime belts requires at least two belts and has several disadvantages compared to an indefinite-lifetime belt system because:

- (1) Launch vehicles for several belts increase costs,
- (2) Several belts would take longer to achieve operational status,
- (3) Communication lifetime is shorter, requiring more frequent replenishment,
- (4) Communication network links are shorter, requiring the use of relay (tandem links) more often, and affording less path diversity.

The lower belt altitudes of the limited-lifetime system do, however, give lower path loss and an attendant slightly higher information capacity.

The major advantages of an indefinite-lifetime belt system come from the greater freedom in design allowing primary attention to be fixed on the belt orbital characteristics as they affect communication lifetime. An adequate system can be provided by a single equatorial belt at an altitude of about 8000 miles. The advantages of such a system over the limited-lifetime system are:

- (1) It may be deployed with a single launch;
- (2) Longer communication lifetime calls for fewer replenishment launches;
- (3) Long links are provided by the higher altitude.

The limited- vs indefinite-lifetime belt may be nothing more than an academic comparison, as the actual question of launching future dipole belts promises to be so thorny that no one may ever come to grips with it. However, it is clear that the requirement of limited-lifetime dipole belts for a communication system has heavy costs associated with it. The full potential of dipole belt communications systems may be examined only in the less constrained context of indefinite-lifetime belts. Although such systems generally would result in lower information capacity due to higher belt altitudes, they would still represent the least expensive dipole belt systems and perhaps the least expensive space-communication systems.

## D. SUMMARY

The general problem of dipole belt design is beyond the scope of this report.<sup>2</sup> We attempt to determine the applicability of dipole belts to government/military communication systems, but very little can be said about dipole belt communication systems in general. We have found it necessary to work out specific examples in order to get a feeling for the potential of dipole belt systems. In this report, we present perhaps the simplest of these specific examples which is interesting from a cost point of view, namely, a communication system which uses only a single, equatorial dipole belt at a sufficiently high altitude (8000 miles) to provide good earth coverage to all regions except the polar caps. This altitude precludes the possibility of a limited-lifetime belt. An 800-kg payload with the type of dipole used in the West Ford experiment will support low data rate communications. The placement of this payload into an 8000-mile equatorial orbit is within the projected capability of the Titan IIIC launch vehicle.<sup>3</sup> Insofar as a specific belt configuration and dipole design were chosen, the results of this work do not apply to dipole belt systems in general. However, the considerations that receive attention, and the approach used in dealing with them can be used as a guide in the design of any dipole belt system. For instance, such computations as information rates, coverage, collision hazard, and optical brightness may be done in the same way for any dipole belt system.

The physical characteristics of the dipole belt used as an example, the " $2r_e$  belt," are summarized in Sec. II, where descriptions of the belt dispensing technique and formation are given. Section II also gives the belt dimensions and lifetime behavior as calculated from several different computer simulations, and evaluation of the optical and collision interference of the belt.

Section III describes the communication coverage possible with the  $2r_e$  belt and suggests a simple network organization plan. In Sec. IV, the communication channel characteristics of the belt are described. Techniques for effectively using such a channel are explained in Sec. V. The communication capacities afforded by the links of the network described in Sec. III with various terminal equipment choices are then calculated and tabulated in Sec. VI. Finally, Sec. VII reviews some of the remaining problems requiring answers before even the  $2r_e$  belt can be realized.

In addition to presenting the manner of the approach to dipole belt systems, this report offers concrete data on the particularly interesting dipole belt configuration studied here. This design is the most economical and certainly represents a lower bound on how well any indefinite-lifetime dipole belt system ought to perform. There may be better belt configurations than those explored here, but at least we offer a point of departure and a basis of comparison for further designs.



## II. DIPOLE BELT PHYSICAL CHARACTERISTICS

The physical characteristics of a dipole belt as an assemblage of orbiting bodies are of interest because of their effect on the communication channel characteristics of the belt (Sec. IV) and on the coverage obtainable (Sec. III). These characteristics also determine other effects of the belt, such as its optical brightness. As a means of describing belt behavior, this section contains a description of a belt formed from a dispenser launched in the equatorial plane at an altitude of about 8000 miles above the earth.<sup>†</sup> The dispensing technique discussed is somewhat similar to that employed in the experimental belt of Project West Ford.<sup>4</sup>

### A. GENERAL BEHAVIOR

The orbit of a copper dipole of small dimensions (0.7 inch in length and 0.007 inch in diameter) about the earth is most noticeably perturbed from a Keplerian orbit by two forces: the earth's equatorial bulge and direct sunlight. A discussion of these, and other perturbations, is contained in Ref. 2. The net effect on equatorial orbits of the major perturbations is that the semi-major axis of the orbit is rotated in the orbital plane. The sunlight force, if its direction is other than parallel to the orbital semi-major axis, also produces changes in the orbit eccentricity; however, the launch conditions for the  $2r_e$  belt may be chosen to keep the angle between the earth-sun line and the orbit axis small.

Perhaps the ideal dipole belt for communications purposes would consist of a large number of dipoles, all having identical orbital elements, but displaced relative to each other along their common orbit so as to maintain a nearly uniform density. Such a belt would permit even large-gain (narrow-beam) antennas to make maximum utilization of the dipoles at any point along the orbit. However, to launch such a belt would require highly sophisticated dispensing techniques; in addition, some influences (such as collisions with micrometeoroid particles) may act selectively on the dipoles so as to permit orbit perturbing forces to influence the dipoles in dissimilar ways.

The dispensing method considered in this report consists of placing all the dipoles into a single (base) orbit, and then imparting them with slightly different velocities to give them dissimilar orbital periods. After a period of time determined by the base orbit period and the maximum dipole velocity difference, the leading and lagging dipoles will meet, and the dipole belt will have been formed. Unfortunately, the dipoles now have different orbital elements, which means that gravitational and solar pressure perturbations will have different effects on different dipoles, causing the dipole orbits to spread apart. Also, the dispensing technique to be described imparts a spin to each dipole which may differ from that of its neighbors, and can be modified by micrometeoroid collisions. The differences in spin direction and rate among the various dipoles cause further dispersion because they affect the average area presented to sunlight and therefore the perturbation due to solar radiation pressure. The degradation in communication performance of the dipole belt due to this dispersion is discussed in Sec. IV.

Another factor in the use of a dipole belt for communications besides the position and velocity dispersion is the influence on coverage of the average orbital elements of the entire belt. It is noted in Sec. III that the communications coverage provided by the belt depends heavily on the belt altitude. We have chosen as an example a single belt in an approximately

---

<sup>†</sup>For brevity, this belt will be called the " $2r_e$  belt," because its mean altitude is two earth radii.

ircular equatorial orbit, with a semi-major axis of three earth radii, or a mean altitude of two earth radii. Such a belt is sufficiently high to provide reasonable earth coverage without introducing excessive path loss; no thorough search for an optimum belt system was conducted in making the selection. A stable orbit, which is one with a nearly constant eccentricity, was chosen in order to maximize the minimum perigee height. A stable orbit is obtained by making the initial orbit (that of the dispenser) eccentric, with perigee located between the earth's center and the projection of the sun (considered as a point) in the orbital plane. As Shapiro<sup>5</sup> has shown, with a proper choice of eccentricity, such an orbit will maintain its center on the earth-sun line projection in the orbital plane, and solar radiation pressure will serve only to rotate the orbit in its plane, but not to affect the eccentricity.

## B. BELT FORMATION

The dipoles of the  $2r_e$  belt are dispensed from a spinning cylinder around which they have been placed in a binder of naphthalene. This material sublimates when heated by the sun and, if this heating is properly controlled, the sublimation and consequent release of dipoles will progress from the outer edge of the cylinder inward. The dipoles of the  $2r_e$  belt<sup>†</sup> are assumed to be placed along circumferences of the dispensing cylinder from a radius of about 12 to 18 inches. The height of the cylinder does not affect orbital behavior for the simulation, so it is unspecified. Its spin axis is perpendicular to the orbit plane. The circumferential dipole placement was chosen rather than the type used in the experimental belt,<sup>4</sup> that is, parallel to the spin axis, because it is desirable for the dipoles to have nearly identical tumbling axes,<sup>‡</sup> a situation which the West Ford dispenser did not seem to provide.<sup>2</sup> If the tumbling axes are nearly aligned, solar radiation pressure effects are more nearly the same for all dipoles, and dispersion due to this source is minimized. The fact that the type of dispenser used in the simulation assures a large anisotropy in tumbling-axis directions follows from the observation of dipole release behavior during the West Ford package checkout process.<sup>2</sup> It was observed there that most dipoles were released at one end first.

A dispenser spin rate of 160 rpm was chosen to give a short belt closure time without causing undue dispersion from the dispensing process. The closure time is the time after launch when the leading and lagging dispensed dipoles meet. For the dispenser described, the maximum velocity change possible for a dipole is the tangential velocity at the maximum radius of the dispenser, or 7.63 meters/sec. The change in orbital period ( $\Delta\tau/\tau$ ) due to a change in orbital velocity ( $\Delta v/v$ ) is given approximately by

$$\frac{\Delta\tau}{\tau} = \frac{3\Delta v}{v} \quad (1)$$

which in this case is 0.005. The closure time is then about 30 days.

The dipoles were assumed to be blackened, i.e., provided with a coating to limit their reflectivity. This blackening reduces the optical reflectivity of the belt and keeps the solar force vector nearly parallel to the earth-sun line, thereby reducing dispersion from sunlight. A figure of 5 percent for reflectivity was used, based on some tests conducted with blackened dipoles.<sup>6</sup>

<sup>†</sup> A summary of  $2r_e$  belt parameters may be found in Appendix B.

<sup>‡</sup> The dipole tumbling motion is the rotation about its center of mass.

### C. BELT DESCRIPTION

In order to obtain an estimate of belt behavior, and to study the effects of some dispensing techniques, several simulations were conducted using an orbit-prediction computer program, modified to treat dipole dispensing and dipole-micrometeoroid collisions by Monte Carlo methods.<sup>2</sup> In each run made, 50 individual dipoles were simulated for a period of about six years, and the resulting belt dimensions calculated as described in Ref. 2. These calculations give, hopefully, a good estimate, but it is only an estimate of expected belt behavior.<sup>†</sup> There are several possible sources of differences between the calculated and actual behavior of the experimental West Ford belt, such as inaccuracies in the dispensing model, curvature of dipoles, and micrometeoroid collisions. There may, in addition, be other factors which would influence a belt such as the  $2r_e$  belt which have not been included.

The results of Figs. 1 through 6 were obtained from three simulation runs for the dispensing conditions given in Appendix B. They differ from each other only in initial eccentricity, micrometeoroid collision model, and initial tumbling axis distribution, as shown below.

<u>Collision Model</u>	<u>Initial Eccentricity</u>	<u>Tumbling Axis Distribution</u>	
No Collision	0.046	$\omega$	( $\pm 0.05\omega$ )
Model A	0.057	$[-\omega, 3\omega]$	( $\pm 0.05\omega$ )
Model B	0.051	$[-\omega, 3\omega]$	( $\pm 0.05\omega$ )

The distribution of tumbling axes is uniform within the range shown ( $\omega$  = dispenser spin rate) and has a component added in each of two directions perpendicular to the spin axis which is uniformly distributed over the interval  $[-0.05\omega, 0.05\omega]$ . Collision model A was chosen to most nearly fit experimental results obtained from satellites,<sup>7</sup> whereas model B used a micrometeoroid flux one-tenth that of model A (see Appendix B).

Figures 1 and 2 show envelopes of the minimum and maximum values attained by the belt cross-section dimensions (in-plane width, out-of-plane width, and area) over its entire girth.<sup>‡</sup> The increase in these dimensions is seen to stabilize at about 10 percent per year within the first two years of belt life. From the results of these and other simulations, it was concluded that the dispensing conditions are of less significance than the micrometeoroid collision model in determining behavior of the belt cross-section dimensions, at least after the first year or so; that is, variations in the dispensing conditions, such as placing the dispenser spin axis perpendicular to the ecliptic instead of to the orbit plane, or using an initial eccentricity of zero or a slightly different distribution of tumbling axes, all gave results similar to those of models A and B of Figs. 1 and 2. The behavior of an actual two-earth-radius belt would probably be contained within the no-collision and the model A curves of the figures inasmuch as these represent two extreme models for micrometeoroid collisions. Note that the actual collision effects encountered must be significantly less than those used in models A and B to produce belt dimensions similar to the collisionless case.

<sup>†</sup> See the comparisons made of theoretical and simulation calculations with actual radar observations of the West Ford belt in Ref. 2.

<sup>‡</sup> The curves obtained from the exact extreme values at 25-day intervals for the first 400 days, and at 100-day intervals thereafter, differ from Figs. 1 and 2 mainly in that a roughly sinusoidal ripple of small amplitude with a period of one year appears in them. Figures 1 and 2 were constructed so as to bound the actual cross-section dimensions.

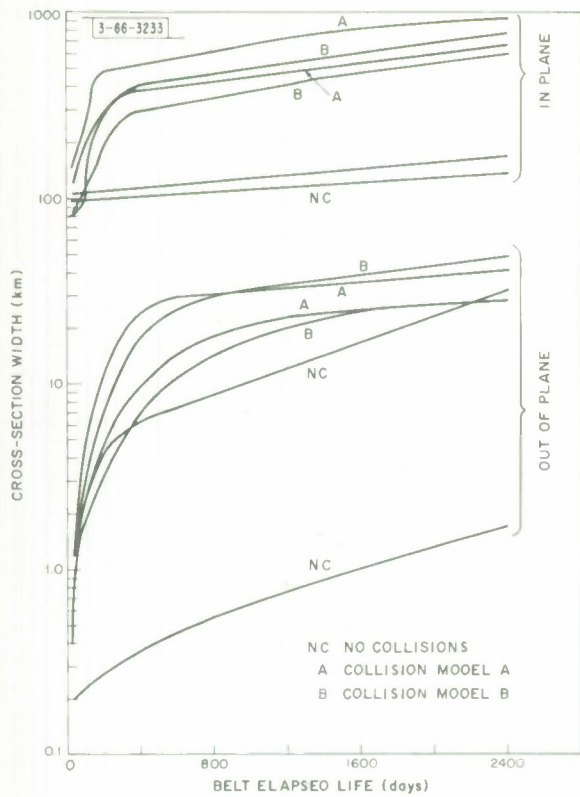
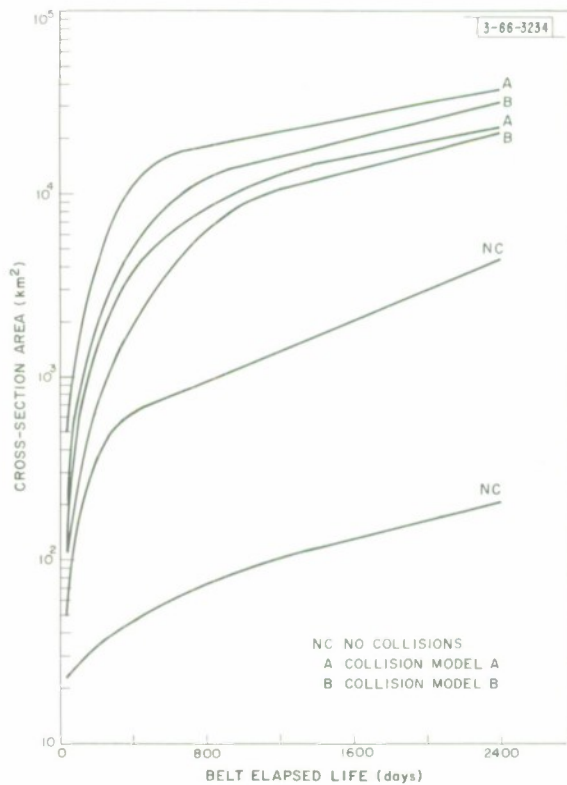


Fig. 1. Extreme values of simulated belt cross-section dimensions.

Fig. 2. Extreme values of simulated belt cross-section area.



The degree of stability attained by the simulation orbits is shown in Fig. 3, where curves of the orbit eccentricity are given for the three simulation cases. The semilatus rectum, mean altitude, and inclination remain essentially constant. Thus perigee height varies between about 1.8 and 1.87 earth radii for the simulated belts.

Cross-section dimensions around the belt are given in Figs. 4 through 6 for the simulated belt using collision model A, for several values of belt age. The true anomaly used in the abscissa of Figs. 4 to 6 is the central angle measured eastward from the location of perigee to a point on the belt. Since the belt orbit is nearly stable, perigee is located approximately on the same meridian as the sun at all times, so that the sun's longitude corresponds to a true anomaly of about zero degrees.

The linear density of dipoles along the orbit is not shown in Figs. 4 through 6 and cannot be inferred from them. In fact, the expected density variations are far less than the corresponding cross-section dimension variations. The linear density is that obtained by projecting all the dipoles onto a common orbit contained within the belt. An estimate of this linear density can be obtained by assuming that individual dipole orbits are circular. In this case, the density of dipole orbital period changes is <sup>2</sup>

$$n(\Delta\tau) = \frac{2N}{\pi\Delta\tau_m} \left[ 1 - \left( \frac{\Delta\tau}{\Delta\tau_m} \right)^2 \right]^{1/2} \quad (2)$$

where N is the total number of dipoles and  $\Delta\tau_m$  is the maximum change in orbital period produced by the dispenser, which is 0.037 hour in our example. Equation (2) assumes the dispenser to be fully packed with dipoles (no central cylinder devoid of dipoles), but to model the dispenser of the  $2r_e$  belt, one can subtract values corresponding to a dispenser whose outer radius equals the inner radius of the simulation model dispenser. In our case, after 90 days, the maximum variation in density is from 0.7 to 1.2 of the average density.

#### D. OPTICAL BRIGHTNESS

The optical brightness of the experimental Project West Ford dipole belt was estimated by several people prior to launch of the belt. These published estimates are listed in W. Liller's article,<sup>8</sup> which presents all the results of the known experimental attempts to measure the optical brightness of the West Ford belt in the early days after dispensing. Liller's comparison of estimated and measured brightness shows that the simple light scattering model used in the calculations was adequate to establish an upper bound on optical brightness.

The hypothetical  $2r_e$  equatorial belt discussed in this report is assumed to consist of 800 kg of dipoles compared to the 19-kg West Ford dipole payload. All other factors being equal, we would expect the  $2r_e$  dipole belt to appear 40 times brighter than the West Ford belt. However, blackened dipoles with optical reflectivity of approximately 5 percent compared to the polished copper West Ford dipoles (reflectivity of 50 percent) largely counteracts the increase in brightness expected from the larger number of dipoles in the  $2r_e$  dipole belt. But the  $2r_e$  dipole belt is expected to have a smaller in-plane spread and hence a smaller subtended angle as viewed from the earth. This factor increases the brightness by about a factor of five. These factors taken together would indicate that the  $2r_e$  dipole belt would appear about 20 times brighter than the West Ford belt.

An upper bound on the optical brightness of the hypothetical  $2r_e$  equatorial belt is plotted as a function of days from dispensing in Fig. 7. The exact dipole and dispenser parameters are

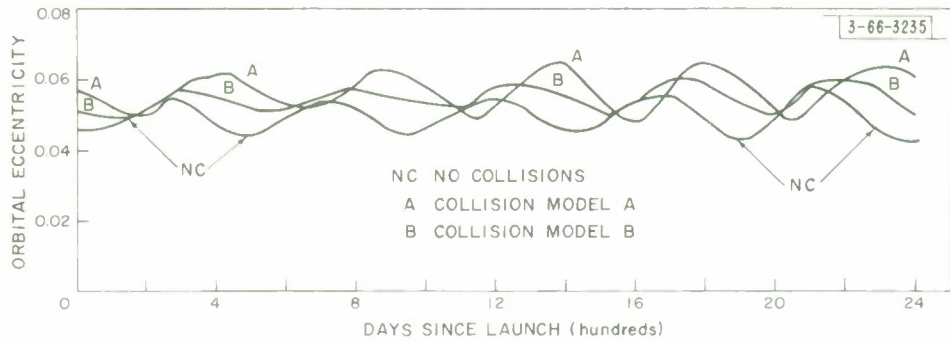


Fig. 3. Variation in eccentricity of simulated belts.

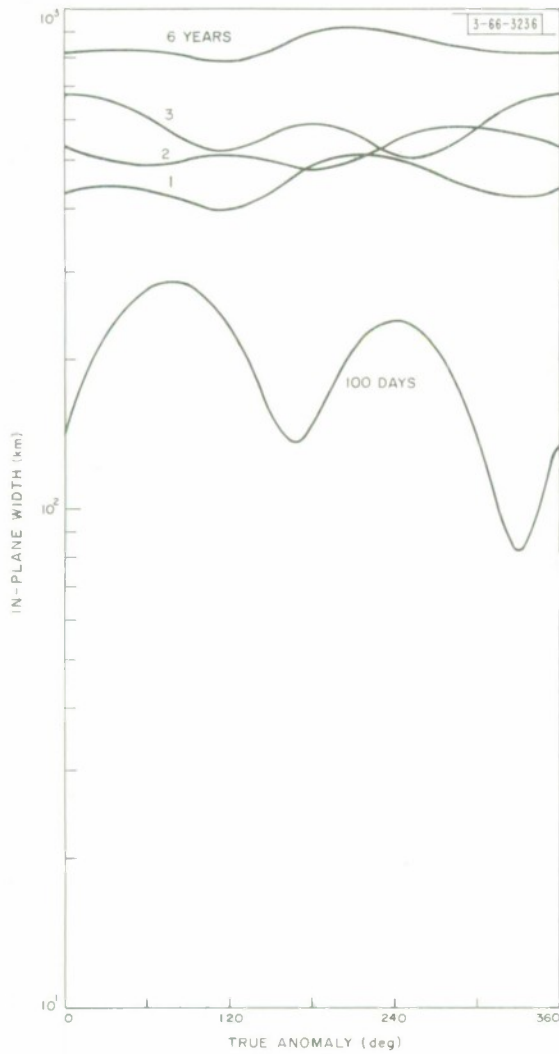


Fig. 4. Simulated belt in-plane dimensions at several stages of belt life.

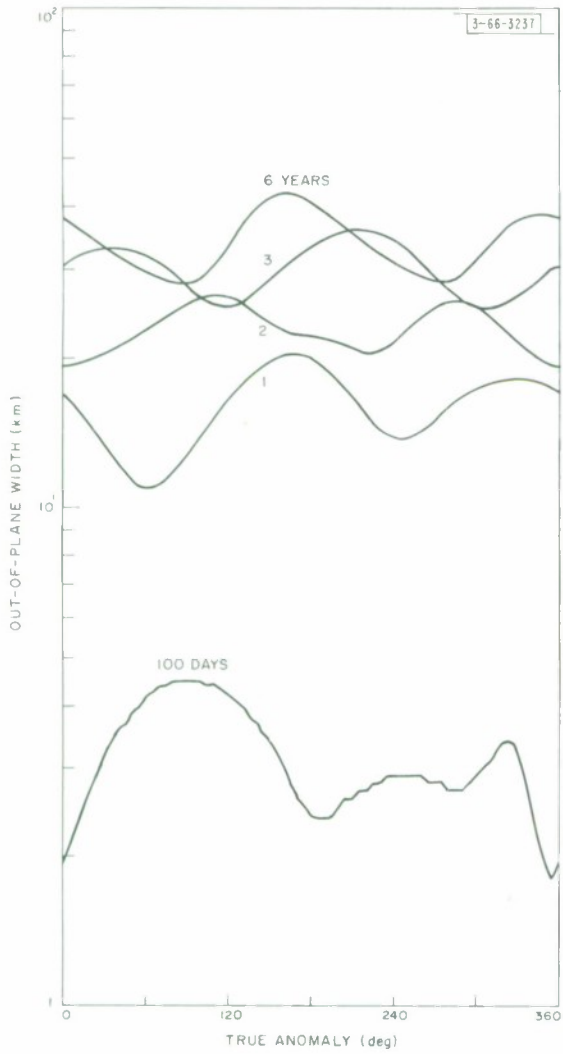


Fig. 5. Simulated belt out-of-plane dimensions at several stages of belt life.

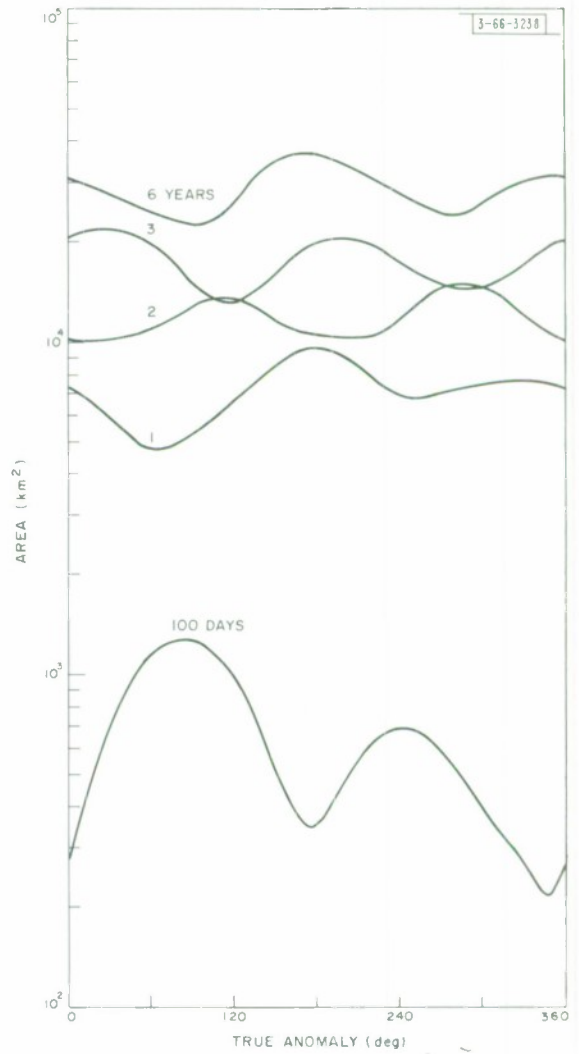


Fig. 6. Simulated belt cross-section area at several stages of belt life.

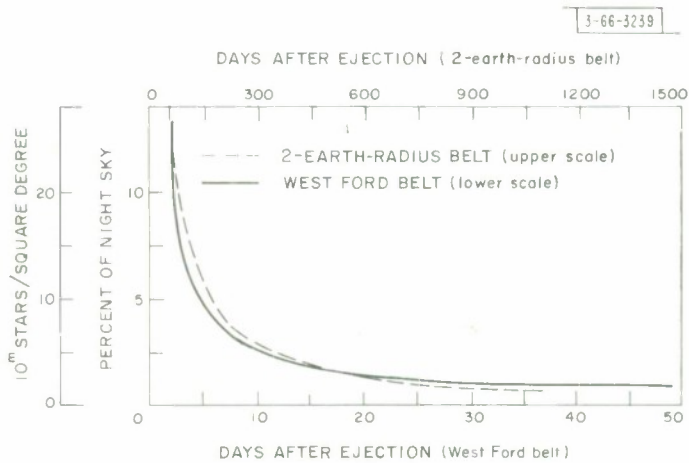


Fig. 7. Brightness of Project West Ford belt compared to two-earth-radius belt.

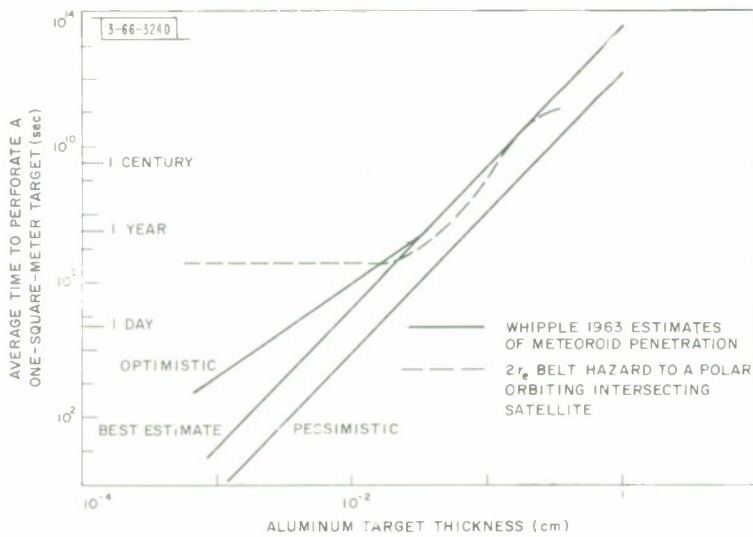


Fig. 8. Meteoroid and dipole penetration of a thin aluminum skin in space.

given in Appendix B. The closure time for this dispenser model is 30 days. The minimum out-of-plane dimension of the belt as a function of time, as found by computer simulation, was used to get this bound on optical brightness. The optical brightness, in units of the number of 10th magnitude stars per square degree, is seen to drop below 5 percent of the night sky background in half a year from dispensing. The night sky background fluctuations are of this order and hence would tend to mask the dipole belt beyond this time.

The brightness of the West Ford belt<sup>8</sup> is also plotted (against the time scale at the bottom of Fig. 7). As a rule of thumb, the brightness of the  $2r_e$  belt would be comparable to the West Ford belt but on a time scale about 30 times longer; that is, the West Ford belt 10 days from dispensing is comparable in brightness to the  $2r_e$  dipole belt 300 days from dispensing.

## E. COLLISION INTERFERENCE

An object of modest size in space can represent a hazard in a collision with another object because relative velocities of several kilometers per second can be attained. Under a hypervelocity impact, a particle with a mass of a few micrograms can penetrate or even perforate metallic plates of the type sometimes used in spacecraft construction. Therefore, it is necessary to consider the hazard a dipole belt, such as the  $2r_e$  belt, represents to other artificial satellites and spacecraft.

Relatively few experimental results have been obtained on hypervelocity impact involving slender filaments, such as the dipoles of the  $2r_e$  belt, and these have been obtained for velocities below those expected during orbital collisions. On the basis of experiments performed at the NASA Ames Research Center<sup>9</sup> using filaments of the type postulated for the  $2r_e$  belt, estimates of the hazard of the  $2r_e$  belt to aluminum-clad satellites can be made as shown in Fig. 8. The experimental impact data and the calculations for obtaining this curve from the data are given in Appendix C. The curve is not extended beyond 40 centuries and 0.4 cm because penetrations of this magnitude require precise alignment of the (straight) dipole with the collision velocity vector (see Appendix C) and are therefore difficult to measure. A maximum penetration of about 2.5 cm is expected with perfect alignment. Figure 8 also shows Whipple's current estimates of the natural meteoroid hazard.<sup>10</sup> Note that the choice of a particular satellite orbit must be made in obtaining the dipole belt hazard because, unlike meteoroids, the dipoles occupy only a small volume of the space about the earth and have roughly a single velocity within any small volume. However, the meteoroids occupy all the surrounding space and have velocities that are generally isotropic in direction. The orbit chosen for the comparison represents an extreme case for conventional satellite launchings and therefore gives a bound to the hazard to any such conventional satellite.

It is seen from Fig. 8 that the natural background and the  $2r_e$  belt represent comparable threats to satellites with conventional aluminum skins in  $2r_e$  polar orbits. Whipple<sup>10</sup> believes his estimate to be in error by no more than one order of magnitude, and the dipole data are believed to be at least as reliable. The dipole hazard will actually be somewhat different than shown by Fig. 8 because of the effects of curvature in the dipoles, although this effect is not expected to make significant changes in the results.



### III. COVERAGE

The physical characteristics of the dipole belt described in the previous section partially determine the communication coverage obtainable. This coverage is also affected by the network equipment used, and by operational and organizational procedures. This section describes the belt visibility parameter calculations and considers a world-wide communication network based on the  $2r_e$  belt.

#### A. BELT VISIBILITY

A basic parameter of dipole belt visibility is the maximum earth-central angle of visibility  $\alpha$  shown in Fig. 9 as the angle between a site on the earth's surface, the earth's center, and a point in space which can be seen from the site using the smallest permissible elevation angle  $e$ . This angle is clearly a function only of  $e$  and the height above the earth of the target point. In fact, from Fig. 9,

$$(h + r_e) \cos(\alpha + e) = A = r_e \cos e$$

or

$$\alpha = \cos^{-1} \frac{\cos e}{a} - e \quad (3)$$

where  $a = (h + r_e)/r_e$  is the height of the point in space above the earth's center, measured in earth radii. From Eq. (3) we can draw several simple conclusions:

- (1) For a fixed value of  $e$ , the maximum value attainable by  $\alpha$  is  $90^\circ - e$ , which occurs for  $a \rightarrow \infty$ ;
- (2) For a fixed value of  $a$ , the maximum value attainable by  $\alpha$  is  $\arccos(1/a)$ , which occurs for  $e = 0$ ;
- (3) For certain regions of interest ( $a \geq 2$ ,  $e \leq 15^\circ$ ),  $(d\alpha/de) \approx -1$ , so that each degree increase in  $e$  produces a decrease of about  $1^\circ$  in  $\alpha$ .

The angle  $\alpha$  is useful in considering visibility because it characterizes two reciprocal situations:

- (1) All surface sites within a circle of angular radius  $\alpha$  from the subsatellite point P can see a point in space of height  $a$  above the earth's center through P, provided they can see within  $e$  degrees of the horizon;
- (2) A site on the surface can see all points at a height  $a$  above the earth's center whose subsatellite points lie within a circle of angular radius  $\alpha$  from the site.

These two visibility circles<sup>†</sup> are shown in Fig. 10, where all sites within the circle about P can see T, and all points at the height of T above the circle about S can be seen from S.

The fraction of the earth's area that lies within a visibility circle of radius  $\alpha$  is given by  $\sin^2(\alpha/2)$ . This relationship is combined with Eq. (3) to give the curves of Fig. 11, where the value of  $\alpha$  corresponding to the percentage area is given on the right ordinate. No pronounced knees exist in the curves of Fig. 11; however, a range of values of belt height between one and three earth radii would appear to offer useful values for a dipole belt. The increase in coverage

<sup>†</sup> The term "visibility circle" will be used to describe either type, as the meaning is clear from the context.

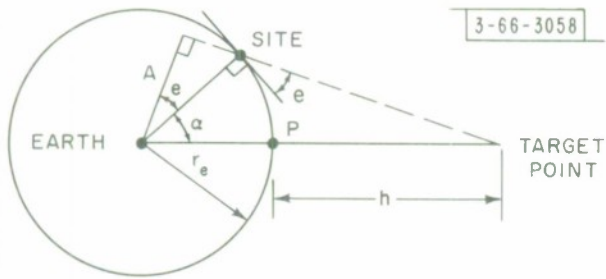


Fig. 9. Earth-space visibility geometry.

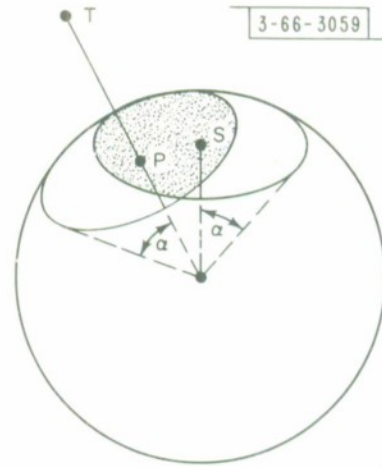


Fig. 10. Visibility circles.



Fig. 11. Visibility angle and area as a function of satellite height.

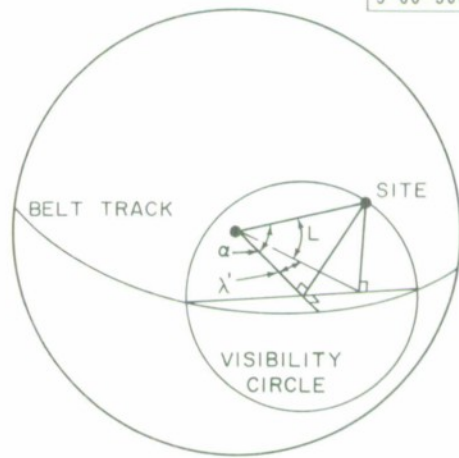


Fig. 12. Visibility circle coordinates.

afforded by higher belts is small, but requires large increases in the communication path; the decrease in coverage of belts lower than one earth radius is severe.

Mutual visibility between two sites via a point on the belt is said to exist if both sites simultaneously hold the point in view. Clearly, this is equivalent to stating that mutual visibility exists only if the visibility circles overlap, and the region of overlap is the region of subsatellite points which provide mutual visibility. If P and S of Fig. 10 are two sites, their region of mutual visibility is shown crosshatched. The mutual visibility region for any pair of sites is not generally of a fixed shape except over short intervals of time because of variations in belt orbit height; also, the track of a belt projected onto the earth's surface is not usually stationary. However, the equatorial dipole belt can be regarded as giving a fixed track which coincides with the equator, and the belt height can be assumed constant at its smallest value to provide a lower bound to mutual visibility. For the  $2r_e$  belt, it is therefore simplest to determine belt visibility regions for the sites of interest, and obtain coverage from their regions of overlap. For non-equatorial belts, visibility must be determined for all possible orientations of the belt with respect to the earth, using the time-varying belt orbital parameters.

The belt visibility region for a single site can be determined by considering a visibility circle constructed about the belt track, i.e., centered on the earth's equator, such that the site lies on the circumference of the circle. With latitude  $L$  measured in the conventional way, and longitude  $\lambda$  measured from the center of the visibility circle, the coordinates of the site are related by

$$\cos \alpha = \cos L \cos \lambda' \quad (4)$$

as shown in Fig. 12. Then  $\lambda'$  is the maximum angle, measured along the belt track (equator) from the meridian of longitude of the site, for which visibility exists from the site to the belt. The belt visibility region for the site is then the interval  $[\lambda - \lambda', \lambda + \lambda']$ , where  $\lambda$  is the longitude of the site. The  $2r_e$  belt described in Sec. II and Appendix B has values between 0.05 and 0.06 for eccentricity with collision model B and an initial eccentricity of 0.051. These two extremes of eccentricity correspond to altitudes at perigee of 1.85 and 1.82 earth radii. If, as in Sec. VI, a value of  $e = 10^\circ$  is used for the radio horizon, and if the minimum altitude value of  $1.82 r_e$  is used, Eq. (3) gives  $\alpha = 59^\circ$ . With such a value for  $\alpha$ , about 13 percent of the earth's surface cannot see the belt, these deprived areas being roughly the regions within the two polar circles.

Figure 13 shows twenty sites which are part of the long-distance trunking network of the United States military forces.<sup>11</sup> This set of sites will be used to demonstrate how the  $2r_e$  belt could satisfy some military communication needs. Only a portion of the trunking network is used in the example because most sites of the complete network are sufficiently near those of the example to exhibit similar visibility and coverage characteristics. The portion of the  $2r_e$  belt visible to the sites is given in Fig. 14, measured in degrees from the prime meridian. The calculation was made on the basis of a circular belt, with  $\alpha = 59^\circ$  as obtained above.<sup>†</sup> A circular belt with a radius equal to the perigee height of the  $2r_e$  belt was used for these calculations because every site will see belt perigee pass through its meridian once a day, thus making the

<sup>†</sup> To include sites in Alaska and Greenland, a reduction to  $7.5^\circ$  was made in the lowest permissible elevation angle for these sites only, giving  $\alpha = 62^\circ$ . Even with  $e = 5^\circ$  sites 19 and 20 cannot be served by the equatorial belt.

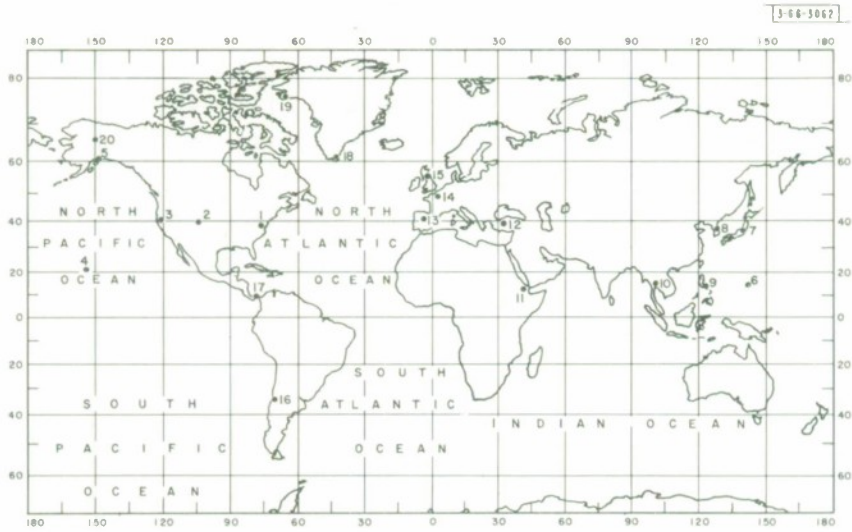


Fig. 13. Network site locations.

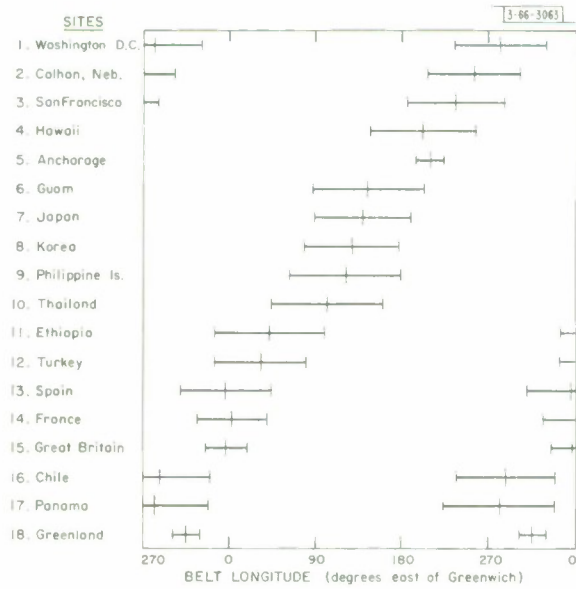


Fig. 14. Dipole belt visibility angles for network sites.

calculation conservative. The visibility arcs obtained when apogee altitude is used in the calculation are not significantly larger than those shown in Fig. 14.

## B. BELT COVERAGE

From the information in Fig. 14, the mutual visibility between pairs of sites of the network of Fig. 13 can be determined, and the communication coverage afforded by the belt is thereby determined. This coverage is shown in Fig. 15 where all sites with mutual visibility via the belt are shown connected by lines. A somewhat clearer presentation of coverage is given in Fig. 16, where totally interconnected sets of sites are grouped within boundaries, and only the links outside these groups are shown.

The coverage in these figures is continuously available as indicated, independent of time of day or year. The  $2r_e$  belt system provides many links for the network; in fact, of the 153 possible links, 69 are direct, 75 require a single intermediate relay, and the remaining 9 require two relays.† Diverse routes are available between all links, usually along several paths with varying relay requirements. These alternate routes frequently make use of identical portions of the belt, so the paths are not necessarily independent.

## C. NETWORK ORGANIZATION

The  $2r_e$  belt can provide adequate communication coverage to a world-wide network of sites. Utilization of all the links described requires that a single site make use of two or more "common volumes," that is, portions of the belt where the antenna beams of two sites intersect and determine a scattering point. These common volumes do not always overlap.

This requirement places the need for two or more transmitting and receiving systems on each site if the network is to be continuously in operation. Alternatively, part of the span of the network can be forfeited by the imposition of operational constraints. One such constraint could be that the operation of links would be determined by a schedule, thereby giving less than full-time coverage, but utilizing every link of the network. Another constraint, somewhat the converse of the one just discussed, would be to use only certain portions of the belt but permit continuous use. Thus, a network of fewer links is the result, but the network can operate continuously.

An example of the application of this latter constraint to the network of Fig. 15 gives the network of Fig. 17. In the constrained network, six segments of the belt have been selected to provide mutual visibility for all the sites located within the visibility circle surrounding that point.‡ Thus any site can be linked with any other site within its same visibility circle by means of one common volume on the belt, namely, the common volume located at the center of the visibility circle. The sites which appear in two circles have the option of being linked with sites in either of these circles, but must use the belt common volume dictated by the circle containing the other site.

A world-wide network can be formed from this system by linking adjacent circles by means of certain sites. For example, sites 8, 9, and 10 of southeast Asia can serve to communicate with sites in both of their visibility circles. If any one of these three sites is capable of simultaneously communicating with sites within both circles, say by using two terminals, it is possible

---

† Use of the apogee altitude in the visibility calculations adds six direct links to this network and reduces by four the number of links requiring a double relay.

‡ Distortions from a circular shape are encountered in showing the visibility circle on a Mercator projection.

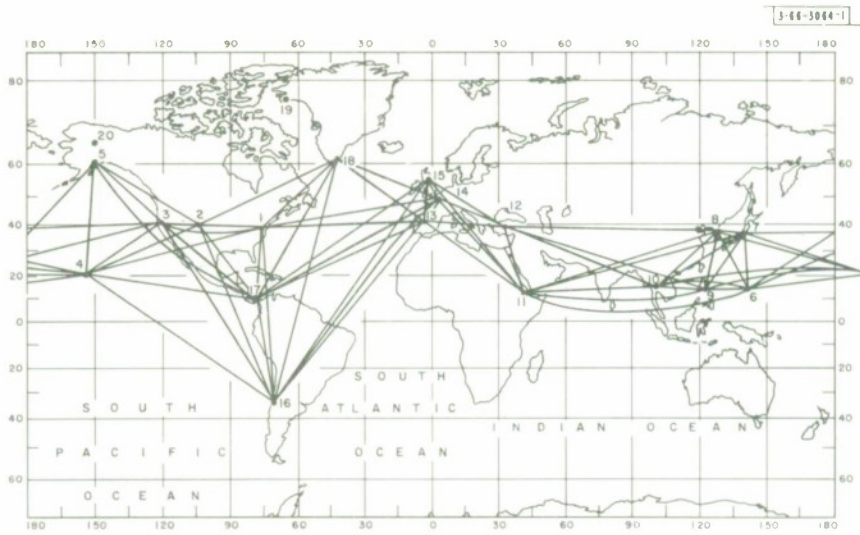


Fig. 15. Coverage map showing network links provided by  $2r_e$  dipole belt. A  $10^\circ$  radio horizon is assumed for all sites except 5 and 18, for which a  $7.5^\circ$  horizon is assumed.

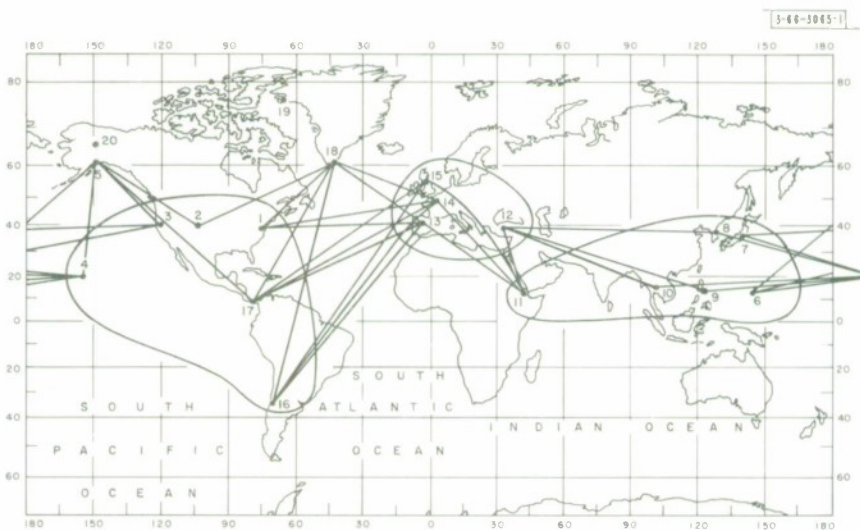


Fig. 16. Simplified coverage map. A  $10^\circ$  radio horizon is assumed for all sites except 5 and 18, for which a  $7.5^\circ$  horizon is assumed.

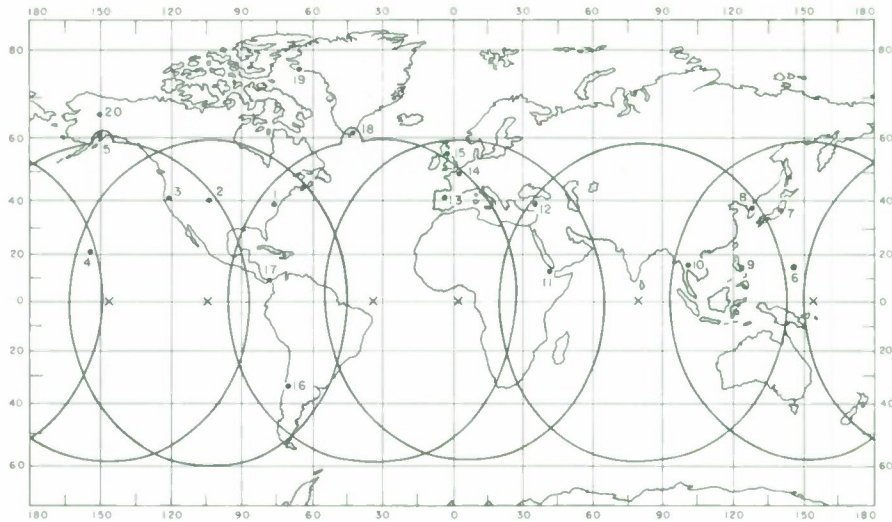


Fig. 17. Regionally centralized network coverage. A  $10^\circ$  radio horizon is assumed for all sites except 5 and 18, for which a  $7.5^\circ$  horizon is assumed.

to provide a single-relay link between Hawaii and the eastern Mediterranean area. If many sites are provided with dual terminals, the number of relays will be minimized and diverse routes provided, but at the cost of the extra equipment.

The regionally centralized system of Fig. 17 can be used to form a network from any group of sites located within its visibility circles. As such, it is fairly adaptable to changes within the network. Any added site, even one of a temporary nature, can join the network by knowing the location of the common volume for its visibility circle. Moreover, because the belt is equatorial and has nearly constant altitude, the actual location of the scatter point will remain within a few degrees of its initial location at any time during the day.



## IV. CHANNEL CHARACTERISTICS

### A. GENERAL

A belt of orbiting dipoles will scatter electromagnetic energy in certain frequency bands very effectively, and so it can be used to transmit signals between widely separated stations. However, it is a very complicated communication channel because its characteristics are changing macroscopically as well as microscopically with time. An RF signal transmitted by a directional antenna pointing at the dipole belt will be scattered in all directions by the dipoles in the antenna beam. A receiving antenna also pointing at these "illuminated" dipoles will receive some of the scattered signal energy. The received signal energy thus depends upon the number of scatterers (dipoles) in the common volume of the two antenna beams. As the belt diffuses (spreads in cross-sectional dimensions) the number of dipoles in the common volume will decrease, eventually prohibiting useful communication. This sort of macroscopic change in channel characteristics takes place on a time scale of many months or even years and is very important in determining the useful communication lifetime of the dipole belt channel.

On the other hand, each individual dipole in orbit is moving with high speed relative to the antennas ( $\approx 3$  km/sec) and may also be tumbling or changing its orientation in some manner with time. Significant changes in dipole orientation probably occur in several tenths, or at the fastest, in several hundredths of a second, since no known mechanism would produce more rapid dipole motions.

Scattering of a signal from a cloud of many dipoles whose relative motions are essentially independent of each other results in a received signal which is microscopically affected in a complicated way. The finite dimensions of the cloud result in propagation paths between transmitting and receiving antennas that have different lengths, implying a spread in signal transmit times due to the "multipath" nature of the channel. A dipole belt channel may have multipath spread in transit time of the order of milliseconds. Also, the high orbital velocity of all the dipoles in the cloud causes a considerable shift of the entire transmitted signal spectrum. But all dipoles are not in precisely the same orbit and hence the dipoles in the cloud have slightly differing vector velocities, resulting in a spread of Doppler shifts of the signals scattered by different dipoles. A relatively small spread in vector velocities of dipoles in the cloud results in a Doppler spread of several kilocycles per second due to the high orbital velocity.

Suppose we transmitted a sinusoidal signal of short duration, say 1 msec or shorter. Since the orientation of a dipole will not change appreciably in this length of time, the scattered signal from each dipole will also be a pulsed sinusoid. The received signal would thus consist of many replicas of the transmitted pulse of different amplitudes, phases, time delays, and Doppler shifts. Suppose the transmitting and receiving antennas are paraboloids 15 feet in diameter and the dipole belt is the  $2r_e$  equatorial belt containing  $2 \times 10^{10}$  X-band dipoles.† A dipole would remain in the common volume of these two antennas for perhaps 20 to 40 sec. Once the belt had closed on itself there would be more than  $10^6$  dipoles actually in the common volume at any instant.

---

† This number of dipoles corresponds to a 1000-kg payload containing 800 kg of 0.7-mil copper dipoles. The placing of this payload into an 8000-mile equatorial orbit is within the projected capability of the Titan III C launch vehicle.

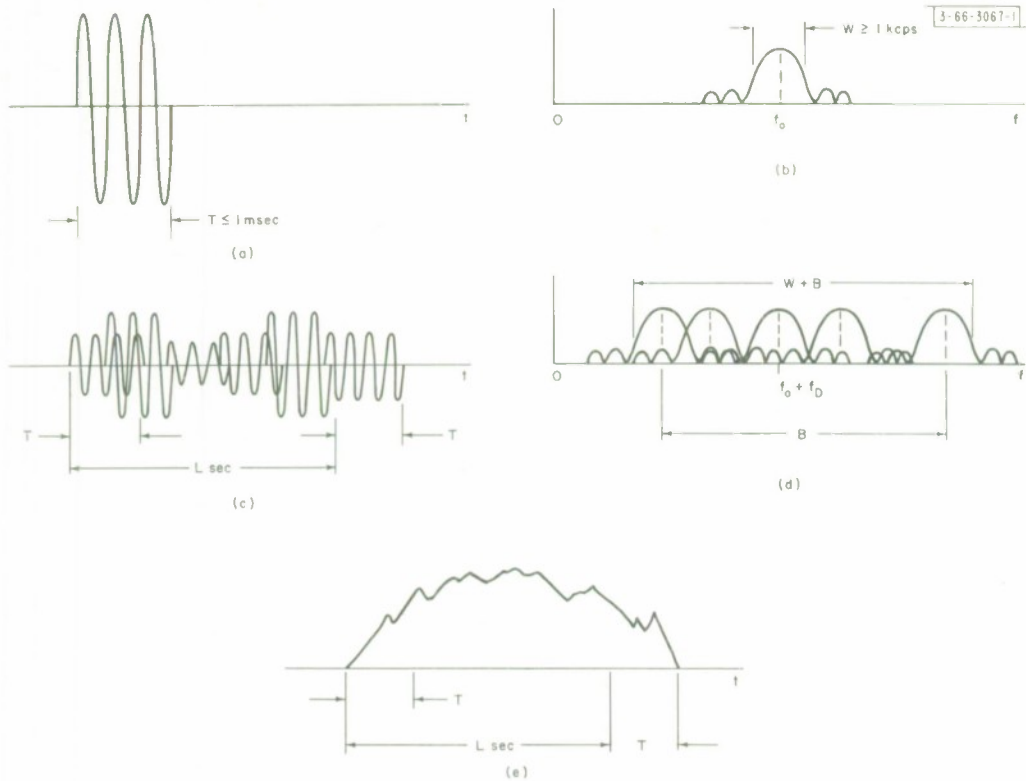


Fig. 18(a-c). Comparison of transmitted and received signals for short pulses ( $T \ll L$ ): (a) transmitted pulse  $s(t)$ ; (b) spectrum of  $s(t)$ ; (c) received signal; (d) received spectrum; (e) envelope of received signal.

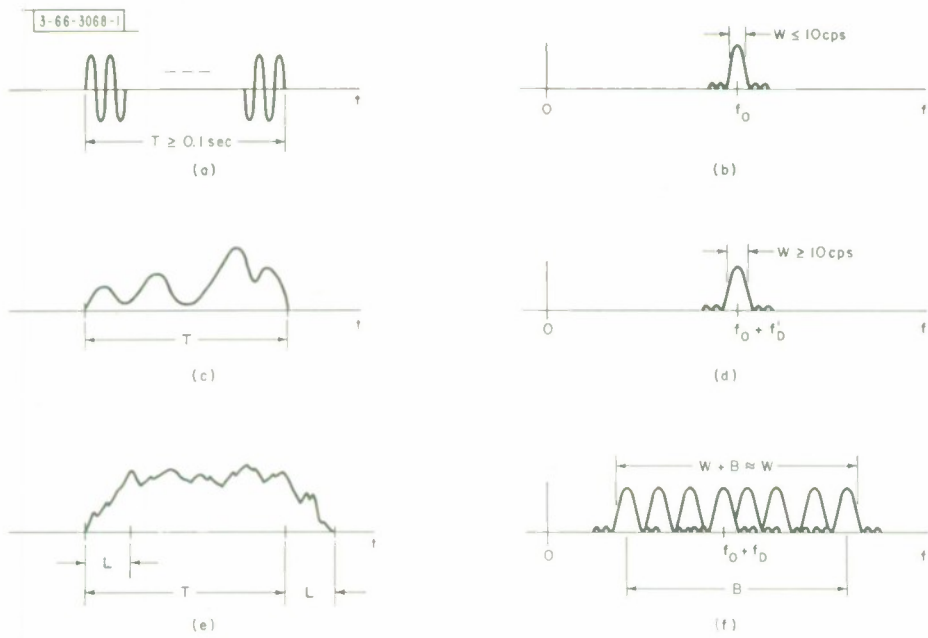


Fig. 19(a-f). Comparison of transmitted and received signals for long pulses ( $T \gg L$  and  $B \gg W$ ): (a) transmitted pulse  $s(t)$ ; (b) spectrum of  $s(t)$ ; (c) envelope of signal scattered from single dipole; (d) spectrum of scattered signal; (e) envelope of received signal; (f) received spectrum.

We therefore cannot hope to recognize any detail of the transmitted waveform in the jumble of pulses that is received.

Even with a pulse length of 0.1 msec, a multipath spread of several milliseconds would result in a received signal which, at any instant, would be the sum of a large number of overlapping RF pulses of different amplitudes, phases, and frequencies, i.e., the received signal would resemble a sample of Gaussian random noise. If the different path delays are approximately uniformly distributed over the interval of multipath spread, we may assume the signal has nearly constant average power in an interval  $T + L$  sec long, where  $T$  is the pulse length and  $L$  is the multipath spread. The total bandwidth of the received signal would be greater than that of the transmitted pulse due to the Doppler spread. If the Doppler shifts due to different dipoles are approximately uniformly distributed in a band  $B$  cps wide, the bandwidth of the received signal will be  $W + B$  cps wide, where  $W$  is the transmitted pulse bandwidth (see Fig. 18).

If we transmitted a sinusoid of longer duration, say  $T = 0.1$  to  $t$  sec, the orientation of a dipole could change significantly in this interval. The signal scattered from a single dipole would now resemble a sinusoid with a slow, random amplitude and phase modulation. Since a multipath spread of several milliseconds is much less than the pulse duration, the spread in transit times results in no significant increase in received signal duration. Each of the randomly modulated sinusoids has bandwidth perhaps as small as 10 to 100 cps (but no smaller because of the modulation). Again assuming Doppler shifts uniformly distributed within a band  $B$  cps wide, the received signal spectrum consists of many overlapping, narrow-band spectra. The received signal again resembles Gaussian noise and the received signal bandwidth is essentially  $B$  cps wide for a Doppler spread of the order of several kilocycles (see Fig. 19).

We will be concerned in this report with only the most rudimentary communication techniques for a channel such as a dipole belt — a rapidly fading, multipath channel. We will consider that the transmitted signal consists of one or several simple, pulsed sine waves separated in frequency so that the spectra of the received signals do not overlap. The received signal due to a simple transmitted pulse of RF energy will be regarded as a sample of Gaussian noise of bandwidth  $B + W$  cps and duration  $T + L$  sec. We make this assumption because of the lack of any further knowledge about the microscopic behavior of orbiting dipoles and also because the large number of dipoles that scatter the signals prohibit us from making any practical use of such microscopic knowledge even if we had any.

In this section, we will estimate the path loss for various transmission paths with the  $2r_e$  equatorial dipole belt from the input of the transmitting antenna to the output waveguide of the receiving antenna. We also estimate the multipath spread  $L$  and the Doppler spread  $B$  for various different hypothetical communication links. These are the only essential parameters which are needed to characterize the dipole belt as a communication channel for the simple model that we have adopted.

There are many other considerations which enter into the design of a communication link which we will not deal with in any detail. For instance, we assume perfect antenna aiming at a chosen point in the dipole belt. This is not unreasonable in a dipole belt system since the only actual tracking that must be done by the antennas is to keep the dipole belt passing through the common volume. If the common volume dimensions are large with respect to the belt cross-sectional dimensions, as in the case of small antennas (10-foot diameter or smaller), antenna aiming is an easy matter. Antenna tracking may be a significant operational problem in a system where a low-altitude (rapidly moving), active satellite repeater must be kept in the antenna beams.

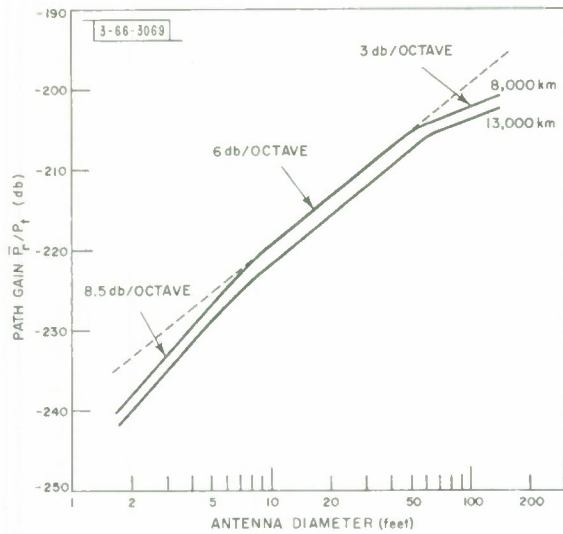
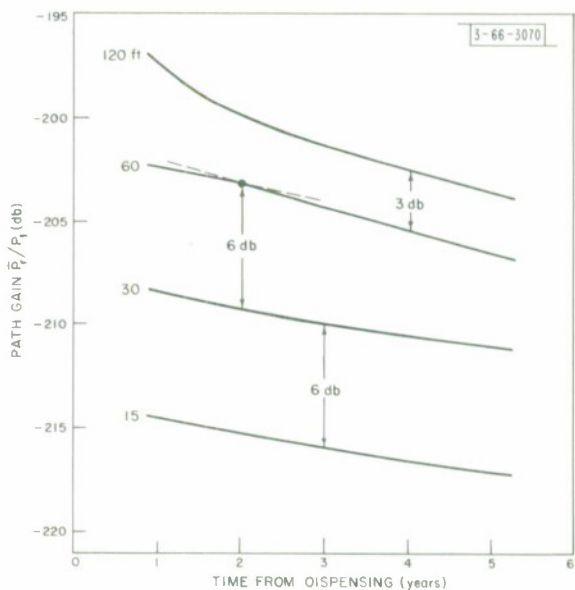


Fig. 20. Path gain vs antenna size for symmetric, equatorial communication links (equal antennas) with station separations of 8000 and 13,000 km, three-year belt dimensions.

Fig. 21. Path gain vs time from dispensing for 8000-km, symmetrical, equatorial links with various antenna sizes.



The single equatorial belt makes acquisition of a common volume easier in the dipole belt system and very little ephemeris and geographical data are needed at communication terminals. The data rates of communication systems using the  $2r_e$  equatorial belt are generally low (of the order of hundreds of bits per second), and thus synchronization of transmitter and receiver after acquisition is not a difficult problem for the simple modulation system discussed in this report.

The path gain of this channel is directly proportional to the number of dipoles included in the common volume of the antenna beams. As the belt spreads in cross-sectional dimensions, the dipole density in the belt decreases, thus increasing the path loss with time until eventually the channel becomes unusable. It should also be noted that antenna size influences path loss (as defined in this study) in a complicated way. First, two small antennas result in a large common volume which may have many times the cross-sectional dimensions of the dipole belt (belt-limited case). If the size of these antennas is now increased slightly, the reduction in the common volume may still result in belt-limited conditions. At some point, as the antenna sizes are increased, the volume containing dipoles will finally be determined by the common volume dimensions (beam-limited case). From this point on, any further increase in antenna size decreases significantly the number of dipoles included in the common volume, thus partially offsetting the effects of increasing antenna size. This is demonstrated in Fig. 20 in which path loss for a long east-west link via the  $2r_e$  dipole belt is plotted against antenna diameter (transmitter and receiver antennas identical). Calculations show that all common volume dimensions are smaller than belt dimensions for antenna sizes of about 60 feet or more, resulting in beam-limited conditions. For antenna sizes between 15 and 60 feet, the out-of-plane belt dimension is smaller than the corresponding common volume dimension, but the large in-plane belt dimension is still larger than common volume dimensions. The abrupt transition from this in-between stage to strict beam-limited conditions can be clearly seen in Fig. 20. Another break in the curve of path loss can be seen as antenna sizes decrease below 10 feet, resulting in strict belt-limited conditions. Figure 20 indicates that it is not worth the cost to increase antenna size much beyond 60 feet for this dipole belt. On the other hand, it is worthwhile to try to employ antennas at least 10 feet in diameter, as reductions in antenna size below this point are very costly in path loss while antenna cost is insignificant. The three-year belt dimensions were used for these calculations.

Since the belt cross-sectional dimensions both increase with time, a communication link using two 60-foot antennas will not be beam limited until three years after dispensing of the dipole belt. Once beam-limited conditions are reached, the scattering volume is just the common volume of the two antenna beams. As the belt disperses, fewer dipoles are included in the common volume, resulting in an increase of path loss with time (dependent on rate of dispersion of the belt). Prior to beam limiting, the scattering volume is increasing as the belt out-of-plane dimension increases, and this effect partially offsets the in-plane dispersion effect. This results in a lower rate of increase in path loss prior to beam limiting. This effect can be seen in Fig. 21 in which we plot path gain vs time from dispensing for an east-west link with two 60-foot antennas.

Another way of viewing Fig. 21 is as follows. From Fig. 20, we see that for strict beam-limited conditions, path gain increases 3 db per octave of antenna size. Prior to strict beam-limiting, path gain increases 6 db per octave with antenna size. Up to two years from dispensing, 15-, 30-, and 60-foot antennas are not yet beam limited and we see a 6-db spacing between these curves on this part of the graph. Beyond two years from dispensing, the 60-foot antennas

are strictly beam limited and we see that the spacing between the 60- and 30-foot curves starts to decrease abruptly. On the other hand, the 120-foot antennas are strictly beam limited beyond two years from dispensing, so we see a 3-db spacing between the 60- and 120-foot curves for this part of Fig. 2.

Only some general conclusions can be drawn from the above discussion. The preferred range of antenna sizes is between 10 and 60 feet. For antennas larger than 60 feet, beam-limited conditions are reached quite soon after dispensing and the extra cost of building such large antennas is not warranted by the slight increase in path gain that they provide. On the other hand, antennas smaller than 10 feet are very costly in path gain but very economical to build.<sup>†</sup>

## B. RECEIVED POWER

A communication link in which signals are transmitted to a receiver by a scattering medium such as a dipole belt may be viewed as a bistatic radar system. We thus write the average received power  $\bar{P}_r$  in terms of the transmitted power  $P_t$  as<sup>12</sup>

$$\frac{\bar{P}_r}{P_t} = \frac{\eta_1 \eta_2 \pi D_1^2 D_2^2}{4^3 R_1^2 R_2^2} \cdot \frac{\sigma}{\lambda^2} \quad (5)$$

where

$\eta_1, \eta_2$  are antenna efficiencies,

$D_1, D_2$  are antenna diameters,

$R_1, R_2$  are ranges to the common volume from antennas 1 and 2, respectively,

$\lambda$  is the wave length at the operating frequency,

$\sigma$  is the average electromagnetic scattering cross section included in the common volume.

For a dipole belt,  $\sigma$  may be expressed as

$$\sigma = N_c \cdot a(\gamma) \quad (6)$$

where  $N_c$  is the number of dipoles in the common volume of the antenna beams and  $a(\gamma)$  is the average scattering cross section of a single dipole with completely random orientation. The bistatic angle  $\gamma$  is defined as the angle between the center lines of the two antenna beams. Reiffen and Check<sup>13</sup> have computed  $a(\gamma)$  for half-wave copper dipoles for circular-to-circular polarization at a frequency of 8000 Mcps as

$$a(\gamma) = [0.0715 + 0.0238 \cos^2 \gamma] \lambda^2 = \lambda^2 k(\gamma) \quad (7)^\ddagger$$

In order to simplify some of the following computations, we assume that the antenna beams are pyramidal with square cross section rather than conical. The antenna beamwidth corresponding to the apex angle of the pyramid approximation is given by

$$\varphi = \sqrt{\frac{4\epsilon}{\pi\eta}} \left( \frac{\lambda}{D} \right) \text{ (radians)} \quad (8)$$

<sup>†</sup> In some situations, antenna size may be constrained by available space, such as in an airborne terminal.

<sup>‡</sup> This is an approximation. The exact curve is plotted in Mack and Reiffen.<sup>14</sup>

where  $\epsilon$  is an efficiency factor. At a range  $R$  from the antenna, the distance across the beam is given by  $R\phi$ .

We can approximate the dipole density in the vicinity of the common volume by

$$\bar{n} = \frac{N}{2\pi(r_e + h) A} \quad (9)$$

where  $h$  is the height of the belt above the earth's surface and  $A$  is the cross-sectional area of the belt in the vicinity of the common volume. If we call the volume containing dipoles  $V$ , we can write  $N_c$  approximately as  $N_c \approx \bar{n}V$ . In the belt-limited case, the common volume has much larger dimensions than the cross section of the belt and so the volume containing dipoles is approximately

$$V \approx A \cdot \min\{R_1\phi_1, R_2\phi_2\} = AR_1\phi_1 \quad , \quad R_1\phi_1 \leq R_2\phi_2 \quad (10)$$

Thus the average received power/transmitted power ratio for belt-limited conditions becomes [using Eqs. (5) to (10)]

$$\left(\frac{\bar{P}_r}{\bar{P}_t}\right)_{\text{belt limit}} = \sqrt{\frac{\eta_1 \epsilon_1}{\pi} \frac{\eta_2 N \lambda k(\gamma)}{64(r_e + h)}} \frac{D_1 D_2}{R_1 R_2^2} \quad , \quad R_1\phi_1 \leq R_2\phi_2 \quad (11)$$

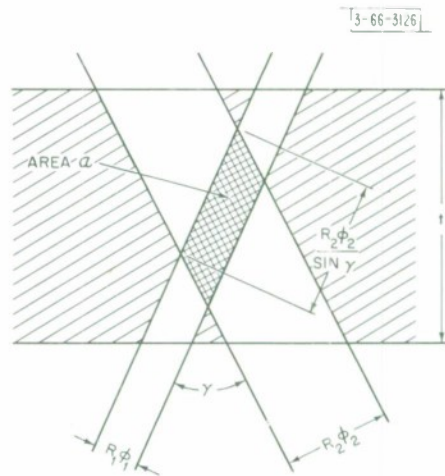
For the beam-limited case in which the entire common volume fits within the dipole belt, we write  $V$  as (see Fig. 22)

$$\begin{aligned} V &= \frac{R_1\phi_1 R_2\phi_2}{\sin \gamma} \min\{R_1\phi_1, R_2\phi_2\} \\ &= \frac{R_1^2 \phi_1^2 R_2\phi_2}{\sin \gamma} \quad , \quad R_1\phi_1 \leq R_2\phi_2 \quad (12) \end{aligned}$$

Then the path gain is

$$\left(\frac{\bar{P}_r}{\bar{P}_t}\right)_{\text{beam limit}} = \sqrt{\frac{\eta_2 \epsilon_2}{\pi} \frac{\epsilon_1 N \lambda^3 k(\gamma)}{16\pi(r_e + h) \sin \gamma}} \frac{D_2}{AR_2} \quad , \quad R_1\phi_1 \leq R_2\phi_2 \quad (13)$$

Fig. 22. Beam-limited scattering volume.



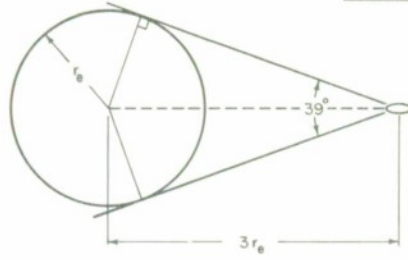


Fig. 23. Geometry of maximum bistatic angle  $\gamma$ .

For the  $2r_e$  equatorial belt, we can see from Fig. 23 that the bistatic angle  $\gamma$  is restricted to  $40^\circ$  or less for any link geometry. We may take  $k(\gamma)$  conservatively as

$$k(\gamma) \geq k(40^\circ) = 0.0855 \quad (14)$$

Furthermore, we can also conservatively take  $R_1 = R_2 = 2.8r_e$ . Since  $k(\gamma)$  can actually range from 0.0855 to  $k(0^\circ) = 0.0953$ , we are conservative in  $k(\gamma)$  by at most  $0.0953/0.0855 (= 0.5 \text{ db})$ . Also, since  $R$  can range from  $2r_e$  to  $2.8r_e$ , are we conservative in using  $R = 2.8r_e$  in the beam-limited equation by  $2.8/2.0 (= 1.5 \text{ db})$ . However, using  $R = 2.8r_e$  in the belt-limited equation can be conservative by as much as  $(2.8/2.0)^3$  which is 4.4 db. This may be too conservative and a more precise estimate of  $R$  may have to be used. Assuming that all antenna efficiencies are 0.5, the wavelength  $\lambda = 0.0375$  meters (corresponding to 8000 Mcps), and the total number of dipoles in the belt is  $N = 2 \times 10^{10}$ , we can write a conservative estimate for  $\bar{P}_r/P_t$  for the beam-limited case as

$$\left(\frac{\bar{P}_r}{P_t}\right)_{\text{beam limit}} \geq 7.38 \times 10^{-13} \frac{D_2}{A} \quad (15)$$

for the  $2r_e$  equatorial belt, where  $D_2$  is the smaller of the two antennas of the link. A conservative but simplified expression can also be derived for the belt-limited case which would have the form

$$\left(\frac{\bar{P}_r}{P_t}\right)_{\text{belt limit}} \geq \text{constant} \times D_1 D_2^2, \quad D_2 \leq D_1 \quad (16)$$

We can see from the Eqs. (15) and (16) that under belt-limited conditions the path gain  $\bar{P}_r/P_t$  is more sensitive to size of the smaller antenna but independent of  $A$ . However, once beam-limited conditions are reached, only the smaller antenna influences path gain, which now decreases with time since  $A$  increases with time, implying the eventual end of the dipole belt as a useful communication channel.

In general, we must write  $N_c$  as

$$N_c = \mathcal{N}V = \frac{N}{2\pi(r_e + h)} \frac{V}{A}$$

in order to estimate path loss. The  $2r_e$  belt has a large in-plane spread  $t$  compared to its out-of-plane spread  $w$ . For a communication link with terminals on the equator and  $R_1 = R_2$ , we can write  $V = \mathcal{A}w$ , where the area  $\mathcal{A}$  is shown in Fig. 22. Thus we write

$$N_c = \frac{N}{2\pi(r_e + h)} \frac{\mathcal{A} \cdot \min\{w, R_1\varphi_1\}}{tw}, \quad R_1\varphi_1 \leq R_2\varphi_2 \quad (17)$$

and the path loss can be estimated fairly accurately in general by computing the area  $\mathcal{A}$ . In this way, we can estimate path loss for the many cases which are neither strictly beam or belt limited. This link geometry is not entirely academic since long links will generally be east-west links rather than north-south links. A computer program was written using Eq. (17) to compute  $\bar{P}_r/P_t$  for many practical antenna combinations and distances between terminals. The results are incorporated in Table I in which  $\bar{P}_r/P_t$  (in decibels) is given for various antenna combinations. The assumed belt dimensions  $t$  and  $w$  corresponded to the three-year belt dimensions.

### C. MULTIPATH SPREAD

The  $2r_e$  dipole belt has an in-plane spread which is much greater than its out-of-plane spread. In addition, the relatively high altitude of the belt restricts the bistatic angle  $\gamma$  to values of  $40^\circ$  at the maximum. We can take advantage of these facts to arrive at a simple approximate formula for multipath spread. For symmetric links, we can see from Fig. 24 that the multipath spread can be written as<sup>†</sup>

$$L = \frac{2D}{c} = \frac{2t}{c} \cos \frac{\gamma}{2} \quad (18)$$

In calculating  $L$ , we may conservatively take the in-plane spread  $t$  corresponding to the maximum spread experienced in three years from dispensing, which is about 700 km. Larger bistatic angles  $\gamma$  tend to decrease  $L$ , so we may take  $\gamma = 0^\circ$  to obtain a conservative estimate of 4.5 msec for the multipath spread after three years.

The largest possible bistatic angle for this dipole belt is  $\gamma = 40^\circ$ , and this results in a multipath spread of 3.5 msec. The dependence of multipath spread on bistatic angle is thus seen to be slight for this dipole belt. The precision of this estimate of multipath spread is entirely adequate for our signal design requirements.

### D. DOPPLER SPREAD

Consider the bistatic radar geometry in Fig. 25 in which a signal is sent from one antenna to another by reflection from a point target  $p$  moving with vector velocity  $\vec{v}$ . The Doppler shift of the received signal can be expressed in terms of the transmitted frequency  $f_0$  as

$$f_D = -\frac{f_0}{c} \dot{l}$$

where  $c$  is the light velocity and  $\dot{l}$  is the time rate of lengthening of the propagation path of the signal. The rate of lengthening of the path from antenna 1 to the target  $p$  is  $\vec{v} \cdot \vec{l}_1$ , where  $\vec{l}_1$  is a unit vector along this path. The path from antenna 2 to the target is lengthening at a rate of  $\vec{v} \cdot \vec{l}_2$ , where  $\vec{l}_2$  is a unit vector along this path. We may thus write the bistatic Doppler shift as

$$\begin{aligned} f_D &= -\frac{f_0}{c} (\vec{v} \cdot \vec{l}_1 + \vec{v} \cdot \vec{l}_2) = -\frac{f_0}{c} \vec{v} \cdot (\vec{l}_1 + \vec{l}_2) \\ &= -\frac{f_0}{c} \vec{v} \cdot \vec{l} \end{aligned} \quad (19)$$

<sup>†</sup> This formula applies strictly only to belt-limited cases, but it may be used as a conservative estimate in other cases.

TABLE I  
 PATH LOSS  $P_t/P_r$  IN DECIBELS FOR VARIOUS ANTENNA COMBINATIONS  
 FOR THREE-YEAR BELT DIMENSIONS, 13,000-km SEPARATION

		Antenna Diameter (feet)											
		2	4	6	10	15	20	30	40	50	60	84	120
Antenna Diameter (feet)	2	240.0											
	4	236.5	231.5										
	6	234.7	229.2	226.8									
	10	232.5	226.7	224.2	221.8								
	15	230.7	224.8	222.3	220.0	218.2							
	20	229.5	223.5	221.0	218.7	217.0	215.7						
	30	227.7	221.7	219.2	217.0	215.2	214.0	212.2					
	40	226.5	220.5	218.0	215.7	214.0	212.7	211.0	209.7				
	50	225.5	219.5	217.0	214.8	213.0	211.8	210.0	208.7	207.8			
	60	224.7	218.7	216.2	214.0	212.2	211.0	209.2	208.0	207.0	206.2		
	84	224.6	218.6	216.0	213.8	212.1	210.8	209.1	207.8	206.8	206.1	204.6	
	120	224.6	218.6	216.0	213.8	212.1	210.8	209.1	207.8	206.8	206.1	204.6	203.1

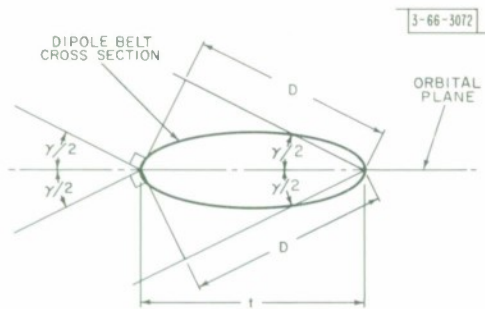


Fig. 24. Geometry of multipath spread calculation.

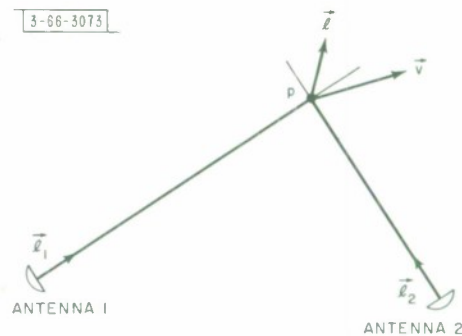


Fig. 25. Bistatic radar geometry.

where we have defined the vector  $\vec{l} = \vec{l}_1 + \vec{l}_2$  which, in general, is not a unit vector. The vector  $\vec{l}$  is called the bistatic orientation vector and it embodies all the pertinent information about the propagation paths concerning the Doppler shift.

It is worth noting that for a symmetrical link, i.e., one in which the propagation paths from each of the antennas to the target are equal,  $\vec{l}$  is perpendicular to the chord line connecting the two antennas. With respect to a satellite communication link in which the target p is in an earth orbit, this means that  $\vec{l}$  is in a radial direction from the earth's center whereas  $\vec{v}$  is generally more nearly tangent to a spherical shell with center at the earth's center.

Fundamentally, Doppler spread arises because the dot product  $\vec{v} \cdot \vec{l}$  in Eq. (19) is not the same for each dipole contained in the common volume. The vector  $\vec{l}$  clearly varies with the location of each point target (dipole) within the common volume. This variation is more significant for large common volumes, which correspond to links with small antennas.

The variation in dipole velocity vectors  $\vec{v}$  within the common volume may be loosely related to the physical dimensions of the dipole belt. Figure 26 illustrates the manner in which the in-plane and out-of-plane belt dimensions can be used to calculate the maximum variation of  $\vec{v}$  within the belt. First, we calculate the maximum angular spread in dipole velocity due to dipole orbits with different eccentricities. In Fig. 26(a), we assume the base orbit or center of the belt is circular with radius  $r_e + h$  and in-plane spread t, and we also approximate a slightly elliptical orbit by a circular one with center displaced from the earth's center. The maximum angular spread in  $\vec{v}$  is easily seen to correspond to orbits of maximum eccentricity for a given in-plane spread t, that is, orbits with perigee at height  $r_e + h - (t/2)$  and apogee at height  $r_e + h + (t/2)$ . Figure 26 shows the maximum radial velocity component  $v_r$  occurring as the eccentric orbit intersects the base orbit, and

$$|v_{r \max}| \approx v_o \delta \approx v_o \frac{t}{2(r_e + h)} \quad (20)$$

The orbit indicated by the solid line in Fig. 26 results in a radial velocity component directed toward the geocenter at p; the orbit indicated by the dashed line corresponds to an oppositely directed radial velocity component at p. The maximum in-plane angular spread in velocity vectors at a point on the base orbit is thus  $\pm\delta$  radians from the tangent to the base orbit at that point. The maximum radial velocity components at other points within the dipole belt due to eccentric dipole orbits can be shown to be

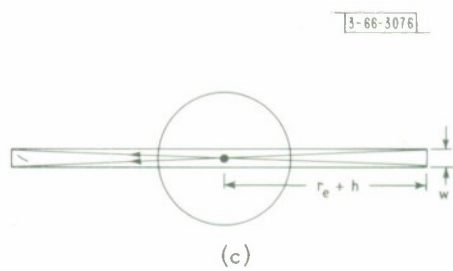
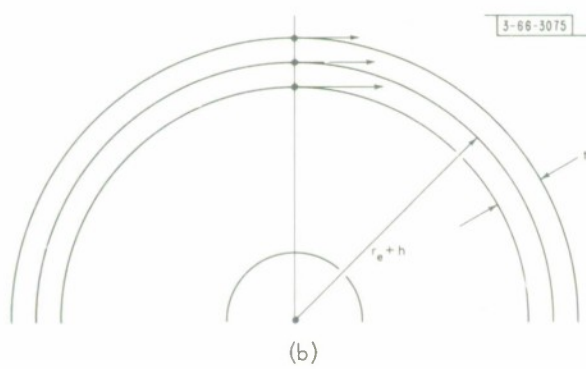
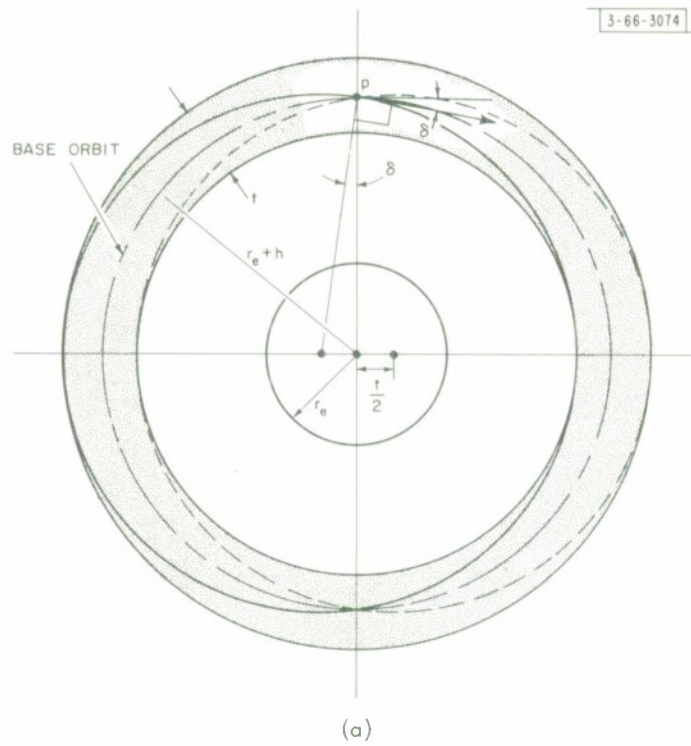


Fig. 26. Variation in dipole vector velocities  $\vec{v}$  due to in-plane and out-of-plane dipole belt spread.

$$v_{r \max}(y) = \pm v_o \frac{\{(\frac{t}{2})^2 - y^2\}^{1/2}}{(r_e + h)} \quad , \quad -\frac{t}{2} \leq y \leq \frac{t}{2} \quad (21)$$

where  $y$  is the distance above the base orbit (negative  $y$  corresponding to points below the base orbit).

The radial velocity spread due to eccentric dipole orbits is very important because the vector  $\vec{l}$  in symmetric links is always very nearly radial, and hence the radial velocity spread contributes strongly to the spread in  $\vec{v} \cdot \vec{l}$  over the common volume.

We may also assume that the in-plane belt spread results, at least in part, from concentric dipole orbits, as shown in Fig. 26(b). Concentric dipole orbits are seen to result in variation of the magnitude of dipole velocities but not to an angular spread in dipole velocities. The orbital velocity of an earth satellite in a circular orbit at a height  $z$  above the surface of the earth is given by

$$v = r_e \left( \frac{g}{r_e + z} \right)^{1/2} \quad (22)$$

where  $g$  is the acceleration due to gravity at the surface of the earth. The difference in orbital velocities corresponding to the innermost and outermost concentric orbits for a dipole belt at a height  $h$  and an in-plane spread of  $t$  km is approximately

$$|\Delta v| \approx \left| t \frac{dv}{dz} \right|_{z=h} = \frac{v_o t}{2(r_e + h)} \quad (23)$$

where  $v_o$  is the orbital velocity corresponding to  $z = h$  in Eq. (22). The spread in velocity magnitude due to concentric orbits is thus seen to be of the same order as the radial velocity components due to eccentric orbits [see Eq. (20)]. Therefore, for symmetric links in which  $\vec{l}$  is nearly always radial from the geocenter, the contribution of the velocity magnitude spread to  $\vec{v} \cdot \vec{l}$  will be of second order compared to the contribution due to radial velocity spread. We thus neglect the effect of concentric dipole orbits within the belt in our computations of Doppler spread.

From Fig. 26(e), we see that the out-of-plane spread  $w$  of the dipole belt will result in an out-of-plane velocity component of at most

$$v_{o.p. \max} = \frac{v_o w}{2(r_e + h)} \quad (24)$$

The out-of-plane belt spread is always much smaller than the in-plane spread and so the out-of-plane velocity components are of second order compared to the radial velocity components. Furthermore, the vector  $\vec{l}$  is very nearly always perpendicular to these out-of-plane velocity components for symmetric links. The out-of-plane belt spread for the  $2r_e$  equatorial belt thus results only in a third-order contribution to Doppler spread and we will henceforth neglect it also.

A general mathematical expression can be derived for the Doppler spread corresponding to a specific point in the common volume. In this development we use the notation and coordinates shown in Fig. 27. Any point  $p$  in the orbital plane can be expressed in terms of the  $x$ - $y$  coordinate axes defined in the figure, or in terms of the  $(\theta_1, \theta_2)$  coordinates. The transformation between  $(x, y)$  and  $(\theta_1, \theta_2)$  coordinates is straightforward and will not be given. The vector  $\vec{l}$  may be written as

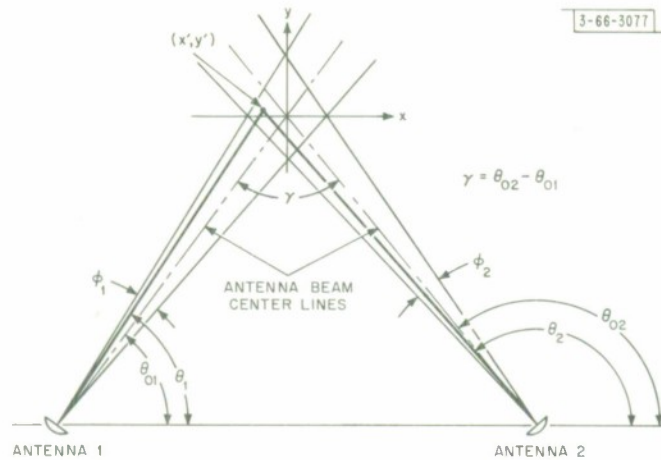


Fig. 27. Geometry used in Doppler spread calculation.

$$\vec{i} = (1/\theta_1) + (1/\theta_2)$$

where  $(a/\theta)$  is used to denote a vector of magnitude  $a$  and angle  $\theta$ . Similarly, we may write the vector velocity of dipoles as a function of the coordinates  $(x, y)$  as

$$\vec{v}(x, y) = (v_0/\psi(x, y))$$

where we have assumed constant magnitude of the dipole velocities but an angle which is a function of position in the belt. Using Eq. (21) we can write  $\psi(x, y)$  as

$$\psi(x, y) = \frac{-x}{r_e + h} \pm \frac{[(\frac{t}{2})^2 - y^2]^{1/2}}{r_e + h} \quad (25)$$

The first term in Eq. (25) gives the angular change in velocity due to the curvature of the orbit. The dimensions of any common volume will be small compared to  $r_e + h$  so the range of  $x$  for which Eq. (25) will be used is small enough to allow us to approximate the arc length along the orbit by the distance along the  $x$ -axis of Fig. 27. The second term of Eq. (25) gives the maximum angular spread due to eccentric dipole orbits.

Now we can write

$$\vec{i} = \left[ 2 \cos\left(\frac{\theta_1 - \theta_2}{2}\right) \angle \frac{\theta_1 + \theta_2}{2} \right]$$

and using the above relations in Eq. (19) results in

$$\begin{aligned} f_D &= -\frac{f_0}{c} (v_0/\psi(x, y)) \cdot \left[ 2 \cos\left(\frac{\theta_1 - \theta_2}{2}\right) \angle \frac{\theta_1 + \theta_2}{2} \right] \\ &= -\frac{2f_0 v_0}{c} \cos\left(\frac{\theta_1 - \theta_2}{2}\right) (1/\psi(x, y)) \cdot \left[ 1 \angle \frac{\theta_1 + \theta_2}{2} \right] \\ &= -\frac{2f_0 v_0}{c} \cos\left(\frac{\theta_1 - \theta_2}{2}\right) \cos\left[\psi(x, y) - \frac{\theta_1 + \theta_2}{2}\right] \quad (26) \end{aligned}$$

This equation can be used to calculate the maximum and minimum Doppler shifts (and hence the Doppler spread) that can be experienced at a point in the dipole belt corresponding to the coordinates  $(\theta_1, \theta_2)$  or  $(x, y)$ . The Doppler spread  $B$  for a symmetric, east-west, communication link in the orbital plane can be found as

$$B \leq \max_{\theta_1, \theta_2} f_D(\theta_1, \theta_2) - \min_{\theta_1, \theta_2} f_D(\theta_1, \theta_2) \quad (27)$$

subject to the constraints

$$\left. \begin{aligned} \theta_{01} - \frac{\varphi_1}{2} &\leq \theta_1 \leq \theta_{01} + \frac{\varphi_1}{2} \\ \theta_{02} - \frac{\varphi_2}{2} &\leq \theta_2 \leq \theta_{02} + \frac{\varphi_2}{2} \end{aligned} \right\} \quad (28)$$

and

The constraints of Eq. (28) simply restrict the maximization and minimizations in Eq. (27) to points inside the common volume. This computation was actually carried out on a digital computer to estimate Doppler spread for a variety of antenna sizes. We present the results of these computations in Table II in which we give the Doppler spread for various antenna combinations.

Antennas on the surface of the earth move in an easterly direction due to the earth's rotation. Since the orbiting dipoles also are moving in an easterly direction, the relative velocity between dipoles and antennas is less than the orbital velocity of 4.56 km/sec (see Appendix B). Using the angular velocities of the antennas on earth and the orbiting dipoles, the relative angular velocity between antennas and dipoles can be computed, resulting in dipole velocity relative to antennas of only 3.135 km/sec. This relative velocity is used for  $v_o$  in computing Doppler spread.

In the special case in which we have two very large antennas which result in a common volume very small compared to the belt cross-sectional dimensions, we may obtain a simple expression for Doppler spread. In this case, we may neglect the curvature of the orbit and the spread in  $\vec{l}$ . Thus taking

$$\vec{l} = (2 \cos \frac{\gamma}{2} \underline{\underline{\frac{\pi}{2}}})$$

and

$$\vec{v} = (v_o \underline{\underline{\pm \delta}})$$

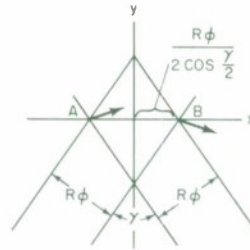
then

$$\begin{aligned} B &\leq \frac{2f_o}{c} 2v_o \cos \frac{\gamma}{2} (1 \underline{\underline{\frac{\pi}{2}}}) \cdot (1 \underline{\underline{\delta}}) \\ &\approx \frac{4f_o v_o \delta}{c} \cos \frac{\gamma}{2} \\ &= \frac{2f_o v_o t}{c(r_e + h)} \cos \frac{\gamma}{2} \end{aligned} \quad (29)$$

Since the neglected effects can only increase Doppler spread, Eq. (29) is a useful lower bound on  $B$  for any case.

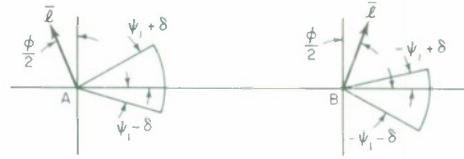
TABLE II  
 DOPPLER SPREAD B (kcps) FOR VARIOUS ANTENNA COMBINATIONS  
 FOR THREE-YEAR BELT DIMENSIONS, 8000-MILE STATION SEPARATION

		Antenna Diameter (feet)											
		2	6	10	15	20	25	30	40	50	60	84	120
Antenna Diameter (feet)	2	8.8											
	6	7.2	7.1										
	10	6.8	6.8	6.8									
	15	6.7	6.7	6.7	6.7								
	20	6.6	6.6	6.6	6.6	6.6							
	25	6.5	6.5	6.5	6.5	6.5	6.5						
	30	6.5	6.5	6.5	6.5	6.5	6.5	6.5					
	40	6.5	6.5	6.5	6.5	6.5	6.5	6.5	6.5				
	50	6.4	6.4	6.4	6.4	6.4	6.4	6.4	6.4	6.4			
	60	6.4	6.4	6.4	6.4	6.4	6.4	6.4	6.4	6.4	6.4		
	84	6.4	6.4	6.4	6.4	6.4	6.4	6.4	6.4	6.4	6.4	6.4	
	120	6.4	6.4	6.4	6.4	6.4	6.4	6.4	6.4	6.4	6.4	6.4	6.4



A POINT OF HIGHEST DOPPLER  
B POINT OF LOWEST DOPPLER

Fig. 28. Doppler spread calculation for equal antenna sizes.



Another special case of interest is

$$\phi = \phi_1 = \phi_2$$

The two points of the common volume contributing the highest and lowest Doppler shift are shown in Fig. 28. At point A we may take

$$\theta_1 = \theta_{01} + \frac{\phi}{2}$$

$$\theta_2 = \theta_{02} + \frac{\phi}{2}$$

and so from Eq. (26)

$$\vec{l}_A = \left[ 2 \cos(\theta_{02} - \theta_{01}) \sqrt{\frac{\pi}{2} + \frac{\phi}{2}} \right]$$

since

$$\gamma = \theta_{02} - \theta_{01}$$

$$\theta_{01} + \theta_{02} = \pi$$

Also, at point A,

$$x_A = -\frac{R\phi}{2 \cos \frac{\gamma}{2}}$$

so that

$$\begin{aligned} \varphi(x_A, 0) &= \frac{R\phi}{2(r_e + h) \cos \frac{\gamma}{2}} \pm \frac{t}{2(r_e + h)} \\ &= \psi_0 \pm \delta \end{aligned}$$

The Doppler shift at A is thus

$$f_D(A) = -\frac{f_0}{c} 2v_0 \cos \frac{\gamma}{2} \left( 1 \sqrt{\frac{\pi}{2} + \frac{\phi}{2}} \right) \cdot \left( 1 \sqrt{\psi(x_A, 0)} \right)$$

which, for small angles  $\phi$  and  $\psi$  becomes

$$f_D(A) \approx -\frac{2f_o v_o}{c} [\psi_o \pm \delta - \frac{\phi}{2}] \cos \frac{\gamma}{2}$$

Since, in general,

$$\psi_o = \frac{R\phi}{2(r_e + h) \cos \frac{\gamma}{2}} < \frac{\phi}{2}$$

for the  $2r_e$  equatorial belt,

$$\psi_o - \frac{\phi}{2} < 0$$

and the maximum Doppler shift occurs for the minus sign taken with the angle  $\delta$ . Hence

$$f_{D \max}(A) = \frac{f_o v_o}{c} \left[ \frac{R\phi}{(r_e + h) \cos \frac{\gamma}{2}} - \phi - \frac{t}{r_e + h} \right] \cos \frac{\gamma}{2}$$

It is easy to show that

$$f_{D \min}(B) = -f_{D \max}(A)$$

so that for a symmetric, equatorial link with equal antennas

$$B \leq \frac{2f_o v_o}{c} \left[ \frac{R\phi}{(r_e + h) \cos \frac{\gamma}{2}} - \phi - \frac{t}{r_e + h} \right] \cos \frac{\gamma}{2} \quad (30)$$

This expression agrees with that derived by Lebow, et al.,<sup>12</sup> for this special case for the experimental West Ford belt.

The Doppler spread can be estimated for north-south links in much the same way and the dominant factor for all but very small antennas is again the velocity spread due to eccentric dipole orbits. In fact, the Doppler spread estimate for east-west equatorial links is conservative in that terminals located elsewhere than on the equator result in smaller magnitudes of  $\vec{v}_r \cdot \vec{l}$ . Such terminals would result in vectors  $\vec{l}$  that would have components in the out-of-plane direction, but the out-of-plane velocity spread is so small that this contribution to B can be neglected. Table II shows that for antennas greater than 10 feet in diameter, the Doppler spread is the same for all links and is given quite accurately by Eq. (29).

## E. RECEIVER SENSITIVITY

The remaining parameter in our simple characterization of a dipole belt as a rapidly fading, multipath channel is the additive noise power at the receiver. The many noise sources that must be taken into account at X-band frequencies are as follows:

Extra-terrestrial	Cosmic or sky noise
	Galactic noise or radio stars
	Sun, moon, and planets
Terrestrial	Atmospheric noise
	Earth radiation
	Condensed water vapor in air and in equipment

Internal

Antenna, feed, and guide losses  
Front-end noise

Radio stars, the sun, the moon, and planets are discrete noise sources in the sky which may be avoided by slight adjustment of antenna aiming angles along the orbit of the dipole belt. It is particularly important to avoid aiming the antenna in the direction of the sun because of its very high noise temperature (6000°K). Significant contributions to the over-all system noise temperature can result even if some of the higher antenna side lobes point at the sun. Cosmic or sky noise is the noise received from the sky background in the direction of the antenna pointing angle. There is some sky noise received from every part of the sky and so this noise component cannot be avoided by slight changes in antenna aiming. At X-band frequencies sky noise is not very significant; it amounts to a noise temperature of about 5°K.

A very important source of receiver noise is molecular absorption of incident microwave energy by oxygen and water vapor in the atmosphere and re-radiation of the absorbed energy as noise. The noise contribution due to oxygen and water vapor depends upon the propagation path length through the atmosphere, which in turn depends on the antenna elevation angle (angle above the horizon). There are many sources of data for finding the antenna noise temperature due to cosmic and atmospheric noise as a function of frequency and antenna elevation angle.<sup>†</sup> At X-band frequencies, the antenna noise temperature varies between 12° and 55°K for antenna elevation angles between zenith (90°) and 10° above the horizon.

The earth is a hot body and its noise temperature at X-band is about 250°K. As the antenna elevation angle decreases, the higher side lobes near the main antenna lobe point at the ground and the receiver temperature increases significantly. The actual noise contribution of the hot earth in the antenna side lobes is a function of the antenna and feed design and is thus difficult to discuss in general terms. It is possible to keep the increase in antenna noise temperature due to low pointing angles down to 15°K for minimum elevation angles of 10° above the horizon.

Another factor which is even more difficult to treat is the effect of a wet antenna surface, radome, or feed horn on antenna noise temperature. Again, this factor is dependent on the particular antenna and feed system design but it is common to observe rises in antenna temperature of 100°K or more when operating low noise receiver systems in rainy conditions, which will be discussed at the conclusion of this section.

The internal noise sources are due to lossy microwave components and the front-end amplifier noise. Microwave systems at room temperatures of about 290°K can achieve attenuations as low as 0.2 db, which would contribute about 15°K to the system noise temperature. The front-end temperature may range from 25° to 50°K for a maser or a liquid helium cooled parametric amplifier, to 100°K for a liquid nitrogen cooled parametric amplifier, to 200°K for an uncooled parametric amplifier.

On the basis of the above figures we calculate the over-all receiver system noise temperature for various receivers and antenna elevation angles in Table III. We assume dry equipment and no rainfall or clouds along the signal propagation path, and no discrete radio noise sources in the antenna beam. The receiver noise power density (single-sided spectrum) can then be calculated as  $N_o$  (watts/cps) =  $kT_r$ , where  $k$  is Boltzmann's constant and  $T_r$  is the over-all receiver system noise temperature.

---

<sup>†</sup> We use R.P. Rafuse (Ref. 15).

TABLE III  
RECEIVER SYSTEM NOISE TEMPERATURES (°K)

Front-End Type	Helium Cooled		Nitrogen Cooled		Uncooled	
	90	10	90	10	90	10
Antenna Elevation Angle (deg)	90	10	90	10	90	10
Sky and atmosphere	12†	55†	12†	55†	12†	55†
Hot earth radiation	–	15	–	15	–	15
Microwave system losses	15	15	15	15	15	15
Front-end	25	25	100	100	200	200
Totals	52	110	127	185	227	285

† Assumes antenna pointing in direction of galactic plane, worst case for sky noise.

## F. SYSTEM OPERATING MARGINS

It is the purpose of this section to examine the variability of all the important parameters of a communication system using a dipole belt channel and to decide on reasonable safety margins in equipment design to overcome some of these variations.

### 1. Dipole Belt

The  $2r_e$  equatorial dipole belt is in a slightly eccentric elliptical orbit and has cross-sectional dimensions that vary considerably around the orbit. Figure 26 shows that the belt cross-sectional area varies over a 2.5:1 range around the orbit. In estimating path loss and multipath and Doppler spread we have conservatively used maximum height and maximum cross-sectional dimensions of the belt at three years from dispensing. The channel parameters will often be better than we assume. For instance, a short link may have a large part of the dipole belt mutually visible to both terminals, and the common volume geometry could be varied over this portion of the belt to obtain the best data rate. However, this sort of variability is not probabilistic, and we use conservative values of channel parameters rather than reliability curves for these parameters.

### 2. Oxygen and Water Vapor Attenuation

The energy absorbed by oxygen and water vapor is re-radiated as noise, and we have examined the resulting effect on receiver noise temperature. The signal attenuation must also be accounted for, since it is appreciable. We take a propagation path with elevation angle  $10^\circ$  above the horizon. The attenuation at X-band due to oxygen and uncondensed water vapor absorption is about 1 db (Ref. 15).

### 3. Rainfall Attenuation

Attenuation of X-band signals propagating through a medium including condensed water vapor is quite severe. For heavy rainfall or heavy fog<sup>16</sup> this attenuation may be as much as 0.1 db/km. A slant propagation path through a cloud layer commonly results in 2-db signal attenuation. Rainfall along a propagation path for an antenna elevation angle of  $10^\circ$  may cause attenuations in

excess of 10 db, with storm centers occasionally resulting in attenuations in excess of 20 db. (Heavy rainfall is taken to be 16 mm/km or more and heavy fog  $2.3 \text{ gH}_2\text{O/m}^3$ . See Ref. 17.)

These figures demonstrate that a rainfall attenuation problem cannot be overcome by power alone. A 20-db power margin is not realistic at this stage of space communications. It seems that several widely spaced terminals ( $\approx 25$  km apart) serving one communication center can use space diversity techniques to advantage in reducing peak rainfall attenuations since storm centers do not generally cover very wide geographic areas. Local weather is an important factor in choosing terminal locations, and the correlation of weather statistics to propagation phenomena is just beginning to receive the deserved attention.

#### 4. Rainfall Noise

Condensed water vapor causes signal attenuation but does not re-radiate this signal power as noise in the X-band region. However, wet radomes, antenna surfaces, and feed horns can result in substantially increased antenna temperature since the water itself is at a rather high temperature. Also, radiation from the earth can be reflected via condensed water vapor in the antenna beam and also will affect the antenna temperature. At the West Ford terminal in Westford, Massachusetts, increases in antenna temperature of as much as  $100^\circ\text{K}$  were observed during rainy conditions.<sup>18</sup>

#### 5. Equipment Degradation

It is not possible to present a reliability curve for equipment degradation for any particular terminal because this is not a probabilistic phenomenon. It is clear that very powerful transmitters and extremely sensitive (low noise temperature) receiver systems are more difficult to keep operating at peak performance. We have already pointed out that very long links will not have a large part of the dipole belt mutually visible and thus they must sometimes be faced with the maximum belt cross-sectional dimensions and height. In general, a short haul link with moderate and hence conservative equipment is much less sensitive to changes in some of the environmental conditions and may be very reliable. On the other hand, a maximum length link using the most advanced terminal equipment may be harder to keep at peak operating conditions and may be less reliable. If we were optimistic, we would probably not include any margin for equipment degradation, but in a conservative mood we would consider a 3-db margin for this factor reasonable.

The usual approach to determining a margin from reliability curves for the various factors mentioned above is a good one. However, we do not have enough knowledge of these factors to construct reliability curves for them. Our only recourse is to adopt some fixed margin which is neither too conservative nor too optimistic. Certainly, more than a 10-db margin would be very costly at this stage, yet less than a 5-db margin would be overly optimistic, since rainfall attenuation alone causes fluctuations in path loss very commonly of this order. In this report, we use the more optimistic margin of 5 db in link calculations.



## V. COMMUNICATION TECHNIQUES

### A. INTRODUCTION

According to the discussion of the characteristics of a dipole belt as a communication channel, we can regard the received signal from such a channel as a sample function of Gaussian noise of duration  $T + L$  sec and bandwidth  $W + B$  cps, where

$T$  = time duration of the transmitted signal,

$W$  = bandwidth of the transmitted signal,

$L$  = multipath spread of the channel,

$B$  = Doppler spread of the channel.

Additive white, Gaussian (thermal) noise also corrupts the received signals. The transmitted signals are always taken to have constant average power over their duration of  $T$  sec so that it is reasonable to assume constant average power of the received signal over its duration of  $T + L$  sec.

The lack of any detailed knowledge of the received signal waveform is a fundamental aspect of this sort of channel. The receiver can only measure the energy of the received signal. The additive noise is a source of inaccuracy in making this measurement. If the power spectrum of the received signal may be taken to be essentially constant over the bandwidth  $W + B$  cps, the estimate of received signal energy may be simply implemented. A bandpass filter restricts the receiver bandwidth to  $W + B$  cps, and the filtered waveform is squared and integrated for a duration of  $T + L$  sec. The final integrator reading is proportional to the energy of the incoming waveform of bandwidth  $W + B$  cps and time duration  $T + L$  sec. The flat spectrum of the received signal together with the flat additive noise spectrum does not require any special emphasis of any part of the spectrum in making our estimate of received signal energy and so the bandpass filter can have a constant gain in the passband.

A simple binary communication system can be constructed for the dipole belt channel by transmitting one of two signals of duration  $T$  sec and bandwidth  $W$  cps to correspond to messages zero or one. If the center frequencies of the signals are separated widely enough so that the received signals of bandwidth  $W + B$  cps do not overlap appreciably in frequency, two energy measuring receivers can be used to differentiate between the two possible transmitted signals. One of the receivers will be estimating the energy (or average power) of a sample of white (thermal) noise of duration  $T + L$  sec and bandwidth  $W + B$  cps; the other receiver will be doing a similar operation on a noise waveform consisting of both the received signal plus the additive thermal noise. Therefore, the two receivers estimate the average power of two noise sources with different average powers, and the decision about the transmitted message is based on the larger receiver output (the larger estimated average power for the sample waveform operated on by the receivers).

Consider expanding a real, bandpass waveform  $x(t)$  of duration  $T + L$  sec in the orthonormal Fourier series

$$x(t) = a_0 + \sum_{n=1}^{\infty} [a_n C_n(t) + b_n S_n(t)] \quad , \quad 0 \leq t \leq T + L \quad (31a)$$

where

$$\begin{aligned} C_n(t) &= \sqrt{\frac{2}{T+L}} \cos 2\pi f_n t \\ S_n(t) &= \sqrt{\frac{2}{T+L}} \sin 2\pi f_n t \quad , \quad f_n = \frac{n}{T+L} = n f_0 \quad . \end{aligned} \quad (31b)$$

The coefficients  $a_n$  and  $b_n$  are given by

$$\begin{aligned} a_n &= \int_0^{T+L} x(t) C_n(t) dt \\ b_n &= \int_0^{T+L} x(t) S_n(t) dt \quad . \end{aligned}$$

For a bandpass waveform having significant frequency content only in the band from  $n_1 f_0$  to  $n_2 f_0$ , the expansion of Eq. (31a) reduces to

$$x(t) = \sum_{n=n_1}^{n_2} [a_n C_n(t) + b_n S_n(t)] \quad , \quad 0 \leq t \leq T+L \quad . \quad (32)$$

The energy of the waveform is given by

$$E_x = \int_0^{T+L} x^2(t) dt = \sum_{n=n_1}^{n_2} (a_n^2 + b_n^2) \quad . \quad (33)$$

If  $x(t)$  is a sample function of Gaussian noise with constant spectral density in the frequency range from  $n_1 f_0$  to  $n_2 f_0$ , the coefficients  $a_n$  and  $b_n$  are statistically independent, Gaussian random variables with equal variances and zero means. The energy  $E_x$  of a waveform  $T+L$  sec long, considered as a random variable, consists of the sum of  $2(n_2 - n_1 + 1)$  squared, independent, identically distributed, Gaussian random variables and thus has a chi-squared probability density of order  $2(n_2 - n_1 + 1)$ .

We will use the above idealized model to characterize the dipole belt channel and receiver operations. Each of the energy measuring receivers of the binary communication system described above will be designed to accept a band of frequencies  $W+B$  cps wide, hence

$$W+B = (n_2 - n_1 + 1) f_0 = \frac{n_2 - n_1 + 1}{T+L}$$

or

$$n_d = n_2 - n_1 + 1 = (T+L)(W+B) \quad . \quad (34)$$

The number  $n_d$  is termed the order of diversity of the received signal  $x(t)$ .

Let us first examine the receiver operating on thermal noise alone. The filtered waveform of bandwidth  $W+B$  cps may be written as  $x(t) = n(t)$ , where  $n(t)$  is a sample function of white, Gaussian noise. Calling the output of this receiver  $E_n$ , we can write the probability density for  $E_n$  as

$$p(E_n) = \frac{(E_n)^{n_d-1} \exp\left[-\frac{1}{2} \frac{E_n}{\sigma_n^2}\right]}{2^{n_d} \Gamma(n_d) \sigma_n^{2n_d}}, \quad E_n > 0 \quad (35)$$

which is a chi-squared density of order  $2n_d$ .<sup>19</sup> The quantity  $\sigma_n^2$  is the variance of the coefficients  $a_n$  and  $b_n$  of the expansion of Eq. (31a) when  $x(t) = n(t)$ . The average value of  $E_n$  is, from Eqs. (33) and (34)

$$\bar{E}_n = \overline{\int_0^{T+L} |n(t)|^2 dt} = \sum_{n=n_1}^{n_2} (\bar{a}_n^2 + \bar{b}_n^2) = 2n_d \sigma_n^2 \quad (36)$$

The average energy of a white, Gaussian noise waveform restricted to a bandwidth of  $W + B$  cps and a time duration of  $T + L$  sec is also given by

$$\bar{E}_n = N_o (W + B) (T + L) = N_o \cdot n_d \quad (37)$$

where  $N_o$  is the spectral density of the white noise (single-sided spectrum).

In the receiver operating on the received signal plus thermal noise, the input waveform, after filtering to bandwidth  $W + B$  cps, may be written as  $x(t) = s(t) + n(t)$ , where  $s(t)$  is the received version of the transmitted signal, assumed to be a sample of white Gaussian noise statistically independent of the thermal noise  $n(t)$ . The probability density of the output  $E_{s+n}$  of this receiver is

$$p(E_{s+n}) = \frac{(E_{s+n})^{n_d-1} \exp\left[-\frac{1}{2} \frac{E_{s+n}}{\sigma_{s+n}^2}\right]}{2^{n_d} \Gamma(n_d) \sigma_{s+n}^{2n_d}}, \quad E_{s+n} > 0 \quad (38)$$

where  $\sigma_{s+n}^2$  is the variance of the coefficients  $a_n$  and  $b_n$  in this case. Since the random processes generating the received signal  $s(t)$  and the thermal noise  $n(t)$  are assumed independent, we write

$$\sigma_{s+n}^2 = \sigma_s^2 + \sigma_n^2 \quad (39)$$

and the average received signal energy is thus

$$\bar{E}_s = \overline{\int_0^{T+L} |s(t)|^2 dt} = 2n_d \sigma_s^2 \quad (40)$$

The decision as to which receiver has the signal plus noise is made on the basis of the larger of the two receiver outputs. Thus errors will be made whenever  $E_n \geq E_{s+n}$ . Since both  $E_n$  and  $E_{s+n}$  are assumed to be chi-squared distributed, an explicit mathematical expression can be derived for the probability of error for this binary communication system as<sup>20</sup>

$$P_e = \frac{1}{\left[1 + \left(\frac{\sigma_{s+n}}{\sigma_n}\right)^2\right]^{n_d}} \sum_{i=0}^{n_d-1} \binom{n_d-1+i}{n_d-1} \left[ \frac{\left(\frac{\sigma_{s+n}}{\sigma_n}\right)^2}{1 + \left(\frac{\sigma_{s+n}}{\sigma_n}\right)^2} \right]^i \quad (41)$$

The probability of error is seen to depend only on  $n_d$  and the ratio  $\sigma_{s+n}^2/\sigma_n^2$  or  $\sigma_s^2/\sigma_n^2$ . From Eqs. (36), (37), and (40), we may write the ratio

$$a = \frac{\sigma_s^2}{\sigma_n^2} = \frac{\bar{E}_s}{N_o \cdot n_d} \quad (42)$$

which turns out to be the signal-to-noise ratio per degree of diversity of the received waveform. A more convenient upper bound on  $P_e$  has been derived by both Kennedy<sup>†</sup> and Yudkin.<sup>21</sup> It is also derived in Appendix B and is

$$P_e < \exp \left[ -\frac{\bar{E}_s}{N_o} L(a) \right] \quad (43)$$

where

$$L(a) = \frac{1}{a} \ln \frac{(2+a)^2}{4(1+a)} \quad (44)$$

and  $a$  is defined in Eq. (42). The function  $L(a)$  is a well-behaved function having a single maximum at  $a \approx 3$ , the value of which is  $L(3) \approx 0.149$ . Therefore, if the order of diversity  $n_d$  of the received signal is such that

$$n_d = n_{d \text{ opt}} \approx \frac{1}{3} \frac{\bar{E}_s}{N_o} \quad (45)$$

then the probability of error can be bounded by

$$P_e < \exp \left[ -0.149 \frac{\bar{E}_s}{N_o} \right] \quad (46)$$

For large  $n_d$ , the asymptotic form of Eq. (41) is exponential, and the exponent agrees with that of Eqs. (43) and (44). This bound on  $P_e$  is thus asymptotically correct in exponent, and the error rate for this channel model depends on both  $\bar{E}_s/N_o$  and  $n_d$ .

Figure 29 shows curves of constant  $P_e$  plotted against  $\bar{E}_s/N_o$  and  $n_d$ . The minimum of the curves with respect to  $n_d$  occur at the maximum value of the function  $L(a)$  in Eq. (44). Therefore, if a fixed  $P_e$  is desired, one can optimize diversity in order to achieve the required  $P_e$  with a minimum  $\bar{E}_s/N_o$ . For this channel model and receiver, the major system design problem hinges on the choice of a set of transmitter signals which result in an order of diversity  $n_d$ , which minimizes  $P_e$  for a fixed  $\bar{E}_s/N_o$  (or minimizes  $\bar{E}_s/N_o$  for a fixed  $P_e$ ).

Our simple model of a dipole belt channel has the obvious advantages of requiring only a small number of gross channel characteristics to specify the model and allowing analysis of simple signalling schemes for the channel. This model has been verified by communication experiments using the experimental dipole belt.<sup>12</sup> It was found that the measured error rates

<sup>†</sup>This bound is presented without derivation by Kennedy in Ref. 22.

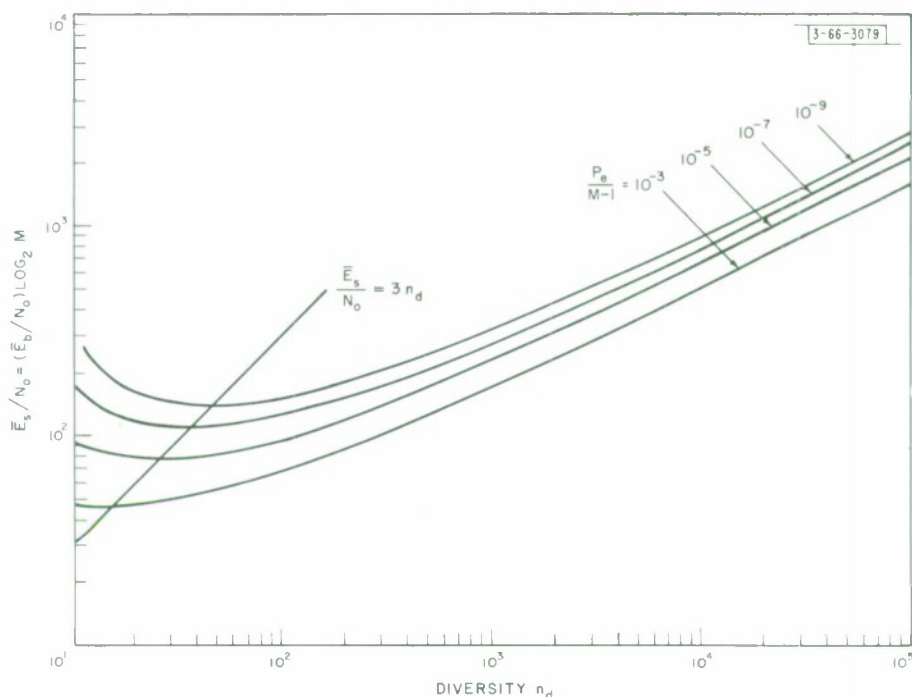


Fig. 29. Curves of constant  $P_e/M-1$  plotted against diversity  $n_d$  and signal-to-noise ratio  $E_s/N_0$ .

agreed reasonably well with those calculated using the simple channel model. The inaccuracy of the calculations based on the model could, to a large degree, be traced to the estimate of multipath and Doppler spread, which determine the diversity  $n_d$ . The difficulty in estimating  $B$  and  $L$  is caused by the nonuniform distribution of Doppler shifts and time delays due to individual dipoles in an actual belt.

## B. M-ARY SYSTEMS

We can use the expressions for probability of error for binary systems given in the previous section to upper bound the probability of error for systems using  $M$ -ary signal alphabets. Suppose a transmitter sends one of  $M$  signals so chosen that the received signal diversity from each is the same and the received signal spectra ( $W + B$  cps wide) do not overlap. Then  $M$  separate receivers can be employed to measure the energy in each of the bands  $W + B$  cps wide in a period  $T + L$  sec long. The decision about which one of the  $M$  signals was sent should then be made on the basis of the largest receiver output (assuming, of course, that each of the signals would suffer equal attenuation in the channel, and the additive noise spectrum was uniform throughout the band covered by the receivers.) We may bound the probability of error for this  $M$ -ary system by

$$P_e(M\text{-ary}) \leq (M - 1) P_e(\text{binary}) \quad (47)$$

where  $P_e(\text{binary})$  is the error rate of a binary communication system given by Eq. (41). We also get an upper bound to  $P_e(M\text{-ary})$  if we have an upper bound to  $P_e(\text{binary})$ . Hence, from Eqs. (43) and (44)

$$P_e(M\text{-ary}) < (M - 1) \exp \left[ -\frac{\bar{E}_s}{N_0} L(a) \right] \quad (48)$$

In an M-ary system, each message corresponds to  $\log_2 M$  bits. If the data rate is R bits/sec, then

$$R = \frac{1}{T_m} \log_2 M \quad (49)$$

where  $T_m$  is the time devoted to the transmission of a single message or  $\log_2 M$  bits. We may write the average received signal energy per information bit  $E_b$  in terms of the energy per  $\log_2 M$  bits as

$$\bar{E}_b = \frac{\bar{E}_s}{\log_2 M} \quad (50)$$

We may thus summarize the bounds on error rate for our channel model as

$$P_e (M\text{-ary}) < (M - 1) \exp \left[ -\frac{\bar{E}_b}{N_o} L(a) \log_2 M \right] \quad (51)$$

where

$$a = \frac{\bar{E}_b \log_2 M}{N_o n_d} \quad (52)$$

$$L(a) = \frac{1}{a} \ln \frac{(2 + a)^2}{4(1 + a)}$$

and

$$n_d = (T + L) (W + B)$$

We can see that if the transmitted signal duration  $T$  is less than  $T_m$ , the time devoted to one message transmission, the transmitter is actually pulsing. When  $T = T_m$ , the transmitter is operating CW and for  $T > T_m$ , several signals must be transmitted simultaneously. Throughout the above analysis it was assumed that the received signals were separated in order to allow measurement of the energy of each of the possible received signals. This implies that a signal at a certain frequency could not be reused for at least  $T + L$  sec, the duration of the received signal. Hence, if  $T_m < T + L$ , two received signals might possibly overlap in time if the same message was to be sent twice consecutively. In this case, the signal separability condition requires that different signal sets be used in sending consecutive messages in order to provide the required  $T + L$  sec between consecutive uses of a signal at a particular frequency.

In practice, a large bandwidth is usually available at X-band so that the location of the set of  $M$  signals can be hopped around the large available bandwidth between messages to prevent overlapping of the received signals. This frequency-hopping technique is easy to accomplish and is a good way to allow several stations to use the same part of the dipole belt as a scattering medium and the same available bandwidth while not interfering with each other appreciably.

Frequency-hopping modulation may also be used effectively with a Gaussian channel which only attenuates transmitted signals without distorting them and in which additive white Gaussian noise also corrupts the received signals. This is a useful model for an active satellite repeater. With the Gaussian channel, the condition of separability of received signals again allows frequency hopping to be used to combat mutual interference of several stations using the same channel.

Thus the form of modulation adopted in this work for systems using a dipole belt channel is basically compatible with an active satellite repeater channel, and has good mutual interference characteristics for both of these channels.

### C. SIGNAL DESIGN

The key problem in choosing the parameters of a modulation system for the dipole belt channel involves the selection of a set of transmitter signals resulting in a good combination of signal-to-noise ratio  $\bar{E}_b/N_o$  and diversity  $n_d$ . The optimum value of diversity was given in the previous section by Eq. (45) as

$$n_{d \text{ opt}} \approx \frac{1}{3} \frac{\bar{E}_b}{N_o} \log_2 M \quad (53)$$

This value of diversity minimizes the required signal-to-noise ratio  $\bar{E}_b/N_o$  to achieve a certain error rate. It would seem reasonable to always attempt to achieve optimum diversity. However, in certain channels with large B and L, the only way to achieve optimum diversity is to use very short pulses as transmitter signals. This results in a low average received signal energy per bit  $\bar{E}_b$  but a higher peak or pulse energy, requiring a high transmitter peak pulse power. In many cases, the peak power required for optimum diversity is impossible to achieve at X-band. Therefore, some other set of signals must be found for which the minimum  $\bar{E}_b/N_o$  is required to obtain a certain error rate while still being consistent with peak and average power requirements of the transmitter.

It is worth illustrating these points with an example. Suppose we have a dipole belt and transmitter and receiver terminals corresponding to the following parameters,†

$$\begin{aligned} \frac{\bar{P}_r}{N_o} &= \text{signal-to-noise ratio} = 29 \text{ db.} \\ L &= 4 \text{ msec} \\ B &= 7 \text{ kcps} \end{aligned}$$

and  $\bar{P}_r$  is the average received signal power. Suppose further that the required error rate is  $10^{-5}$  or less. We wish to specify the transmitter signal duration T and bandwidth W for a binary modulation system which will maximize the data rate for this particular communication link.

If a simple pulsed sinusoid of duration T is sent, the bandwidth of such a signal is approximately  $W \approx 1/T$  cps. Assuming we can adjust T to achieve optimum diversity, the error rate could be upper bounded as in Eq. (46). Solving the inequality

$$10^{-5} < \exp \left[ -0.149 \frac{\bar{E}_s}{N_o} \right]$$

for  $\bar{E}_s/N_o$  we get

$$\frac{\bar{E}_s}{N_o} > 77 = (18.9 \text{ db})$$

The signal-to-noise ratio  $\bar{E}_s/N_o$  can be expressed as

---

†These parameters are consistent with the  $2r_e$  belt and two medium-sized terminals (15- to 30-foot antennas).

$$\frac{\bar{E}_s}{N_o} = \frac{\bar{P}_r}{N_o} T_b$$

where  $T_b$  is the time taken to transmit a single information bit. For a binary system, the data rate  $R = 1/T_b$ . Hence

$$\frac{\bar{E}_s}{N_o} = \frac{\bar{P}_r}{N_o} \frac{1}{R} > 77 (= 18.9 \text{ db})$$

or

$$R < \frac{\bar{P}_r}{N_o} \frac{1}{77} \approx 10 \text{ bits/sec} (= 10 \text{ db})$$

From Eqs. (45) or (53), we calculate that the optimum diversity is

$$n_d \text{ opt} \approx \frac{1}{3} \cdot 77 \approx 26$$

But the minimum diversity corresponding to a given B and L is

$$n_d \text{ min} = (\sqrt{BL})^2$$

For the values of B and L in this example,

$$n_d \text{ min} = 40$$

We are thus forced to operate with a larger value of  $n_d$  than optimum, implying a larger value of  $\bar{E}_s/N_o$

Suppose we operate at the minimum diversity of  $n_d = 40$ . From Fig. 29, we see that we must have

$$\frac{\bar{E}_s}{N_o} \geq 80$$

and so

$$R \approx 10 \text{ bits/sec}$$

$$T = 1 \text{ msec}$$

and

$$\frac{T_b}{T} = 100$$

If the average transmitter power is 1 kw or more, this duty cycle implies a peak or pulse power of 100 kw or more, which is close to the maximum power level currently achievable at X-band. A lower duty cycle is thus desirable.

If the pulse length is increased to 13.5 msec, the diversity is increased to  $n_d = 125$ , which seems far from optimum. We see from Fig. 29 that an error rate of  $10^{-5}$  can be achieved with this diversity and a value of  $\bar{E}_s/N_o = 102$  which is only 1.2 db worse than the minimum signal-to-noise ratio of 77 to achieve this error rate. The resulting data rate is

$$R \approx \frac{\bar{P}_r}{N_o} \frac{1}{102} = 7.5 \text{ bits/sec}$$

and the duty cycle is thus decreased to

$$\frac{T_b}{T} = \frac{1}{RT} \approx 10$$

This sort of duty cycle is much more reasonable, and it has been achieved at a very slight cost in data rate.

Further increasing the pulse length  $T$  to 75 msec increases the diversity to  $n_d = 550$ , resulting in a required signal-to-noise ratio of  $\bar{E}_s/N_o = 175(22.4 \text{ db})$ , a data rate of

$$R \approx \frac{\bar{P}_r}{N_o} \frac{1}{175} = 4.5 \text{ bits/sec}$$

and a duty cycle of

$$\frac{T}{T_b} \approx 3$$

If the transmitter is constrained to operate continuously (CW) then the duty cycle is  $T/T_b = 1$ . We must find a value of  $R = 1/T_b = 1/T$  which results in a signal-to-noise ratio

$$\frac{\bar{E}_s}{N_o} = \frac{\bar{P}_r}{N_o} \frac{1}{B}$$

and a value of diversity

$$n_d = \left(\frac{1}{R} + L\right) (R + B)$$

which are consistent with the relationship between these quantities plotted in Fig. 29. The results are

$$R = 2.0 \text{ bits/sec}$$

$$\frac{\bar{E}_s}{N_o} = 400 (= 26.0 \text{ db})$$

$$n_d = 3500$$

In this example, the data rate for CW transmitter operation is one-fifth the data rate corresponding to minimum diversity.

The ratio  $\bar{P}_r/N_o$  may be related to terminal parameters as

$$\frac{\bar{P}_r}{N_o} = P_t \left(\frac{\bar{P}_r}{P_t}\right) \frac{1}{N_o} \tag{54}$$

where the path loss  $\bar{P}_r/P_t$  includes the antenna gains of each terminal and is derived in Sec. IV. The quantities  $\bar{P}_r/P_t$ ,  $B$ , and  $L$  thus depend upon the dipole belt, geometry of the communication link and antennas. The average transmitter power  $P_t$  and receiver sensitivity  $N_o$  (or temperature  $T_r$ ) are purely terminal parameters. The modulation system parameters are  $M$ ,  $P_e$ ,  $T$ , and  $W$ .

It is worth pointing out that in a transmitter operating with a very low duty cycle, the power supply must store energy for a long time between pulses. This may represent a difficult design problem. However, this problem may be avoided in some cases by breaking the single pulse corresponding to a signal into several shorter pulses equally separated in time. The only factor that must be checked is the resulting diversity of the received signal which is the sum of the diversity of the received signals due to the shorter pulses.

To illustrate this point, consider the 13.5-msec pulse length case in the above example which resulted in a duty cycle of 10 and a data rate of 7.5 bits/sec. A single 13.5-msec pulsed sinusoid may be sent every  $1/7.5 = 133.3$  msec, resulting in a diversity of 125. The transmitter power supply would have to store energy over a period of  $133.3 - 13.5 = 120$  msec, and this condition might lead to some difficult filtering problems. An alternate signal design might be to require the transmitter to send two 4.7-msec pulses every 133.3 msec which would lead to a diversity of 62 from each pulse, or a total diversity of 124. The power supply would only have to store energy over a period of  $(133.3/2) - 4.7 \approx 62$  msec. In this case the duty cycle changes to  $133.3/(2 \times 4.7) = 14$  which may or may not be acceptable. However, as we have shown, in many cases in which the data rate is low, a long pulse can be broken into many more than two shorter pulses while keeping both the received diversity and the duty cycle the same.

The dipole belt channel is not considered a high data rate channel, especially if small, transportable terminal equipment is used. The low data rates usually lead to diversities much larger than optimum if there is a limit to the achievable duty cycle or transmitter peak (or pulse) power. Since there is no way to reduce the diversity except by choice of pulse length, the system has to cope with a higher diversity, and signals should be chosen to maximize the data rate for a given error rate while also satisfying peak and average transmitter power requirements.

In some cases, one finds that a relatively high data rate system (resulting from large terminals) may have less than the optimum diversity if simple pulsed sinusoids are considered as signals. One can always increase the diversity as much as desired by using more complex transmitter signals for which the time-bandwidth product  $TW > 1$ . Consider the following example in which

$$\frac{\bar{P}_r}{N_o} = 46 \text{ db}$$

$$B = 2 \text{ kcps}$$

$$L = 3 \text{ msec}$$

$$M = 2$$

$$P_e < 10^{-5}$$

Assuming we can achieve optimum diversity we first calculate the maximum possible data rate for this situation as

$$R_{\max} \approx \frac{\bar{P}_r}{N_o} \left( \frac{\bar{E}_s}{N_o} \right)^{-1} n_{d \text{ opt}} = 520 \text{ bits/sec}$$

which for CW transmission corresponds to a pulse length of

$$T = \frac{1}{R} = 1.9 \text{ msec}$$

This pulse length, however, results in a diversity of  $n_d = 15$  which requires a signal-to-noise ratio of  $E_s/N_o = 84$  to achieve  $P_e < 10^{-5}$  rather than the minimum assumed ratio of 77 corresponding to  $n_{d \text{ opt}} = 26$ . Instead of the simple pulsed sinusoid of 1.9 msec with  $TW \approx 1$ , consider a signal with  $T = 1.9$  msec consisting of a sinusoid with phase reversals every 1.9/5 msec.<sup>†</sup> The bandwidth of this signal is approximately  $W \approx 5/T$  and hence the diversity for such a signal would be

$$n_d = (T + L) \left( \frac{5}{T} + B \right) = 26.3$$

which is close enough to optimum diversity to allow system operation with  $E_s/N_o = 77$ , as assumed for the  $R = 520$  bits/sec. The point of this example is that received diversity can always be increased by using signals with  $TW > 1$ , and one need never operate with less than the optimum diversity. Since no signals provide  $TW < 1$ , cases will arise in which diversities much larger than optimum will have to be accepted.

---

<sup>†</sup> The diversity could also be increased by sending several pulses with different frequencies simultaneously, but the transmitter signals no longer have a constant envelope. See Kennedy and Lebow<sup>22</sup> for a detailed discussion on how to increase diversity.



## VI. COMMUNICATION LINK DESIGN

### A. GRAPHICAL DETERMINATION OF MODULATION PARAMETERS

Given a particular link geometry and a pair of terminals, one must still define the modulation system parameters which maximize the data rate for the specific link. We usually start the signal design problem with  $\bar{P}_r/N_o$ , B, L, a required error rate  $P_e$ , and perhaps an alphabet size M which is strongly related to the complexity of the signal processing equipment. As a trial design we could assume optimum diversity which implies a data rate satisfying [using Eq. (49)],

$$\left(\frac{\bar{E}_s}{N_o}\right)_{\min} = \frac{\bar{P}_r}{N_o} T_m = \frac{\bar{P}_r}{N_o} \frac{\log_2 M}{R} \quad (55)$$

The assumed diversity  $n_{d \text{ opt}}$  together with B and L implies a value for the pulse length T for simple pulses in which  $TW \approx 1$ . The duty cycle dc is then computed as

$$dc = \frac{T_m}{T} \quad (56)$$

and checked against the peak power requirements of the transmitter. At this point there are three possibilities:

- (1)  $dc < 1$
- (2)  $1 \leq dc \leq DC$
- (3)  $DC < dc$

where DC is the maximum allowable value of the duty cycle dc

Case 1 implies that the diversity is less than  $n_{d \text{ opt}}$ , necessitating only more complex signals with  $TW > 1$  to achieve  $n_{d \text{ opt}}$  and a suitable signal design. Case 2 also implies that a suitable solution to the signal design problem has been found since the duty cycle to achieve  $n_{d \text{ opt}}$  is less than the maximum allowable one. Case 3 implies that our trial design was too optimistic and our assumption of  $n_{d \text{ opt}}$  has led to an unsatisfactory duty cycle. Another trial signal design may then be carried out as follows, starting with a lower data rate.

- (1) With the new value of R calculate  $T_m = \log_2 M/R$ .
- (2) Find the actual signal-to-noise ratio

$$\frac{\bar{E}_s}{N_o} = \frac{\bar{P}_r}{N_o} T_m = \frac{\bar{P}_r}{N_o} \frac{\log_2 M}{R}$$

- (3)  $T = T_m/DC$ .
- (4)  $n_d = (T + L)(1/T + B)$  (simple pulses in which  $TW \approx 1$ ).
- (5) Using  $n_d$ , M, and the desired  $P_e$ , use Fig. 29 to find the required signal-to-noise ratio  $(\bar{E}_s/N_o)^*$ .
- (6) Compare the actual  $\bar{E}_s/N_o$  with  $(\bar{E}_s/N_o)^*$

If the required signal-to-noise ratio  $(\bar{E}_s/N_o)^*$  found from M,  $n_d$ , and  $P_e$  is larger than the actual value  $(\bar{P}_r/N_o) T_m$ , then a lower data rate must be assumed and the trial design carried through again. If the actual  $\bar{E}_s/N_o$  exceeds  $(\bar{E}_s/N_o)^*$ , the data rate should be increased slightly before carrying out the trial design again. This procedure will converge to data rate R and a pulse length T which satisfy

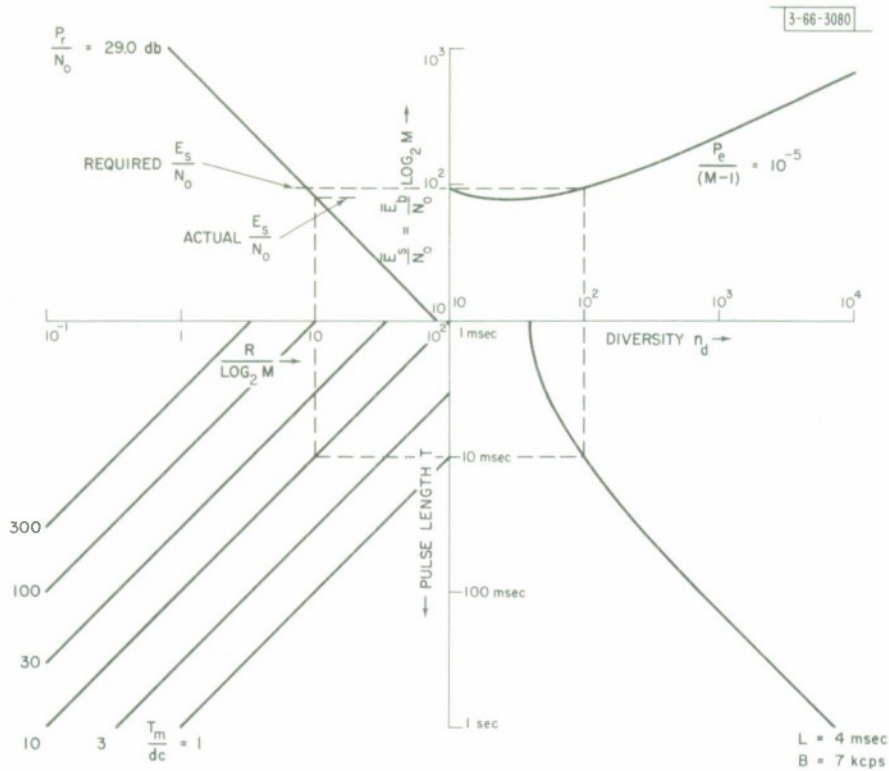


Fig. 30. Set of design curves for the example of Sec. V.

$$\frac{T_m}{T} = DC$$

and

$$\frac{\bar{P}_r}{N_0} \frac{\log_2 M}{R} = \left( \frac{\bar{E}_s}{N_0} \right)^* \quad (\text{from } n_d, M, \text{ and } P_e)$$

In Fig. 30 we present a set of design curves which allows the trial designs to be performed graphically. The curves correspond to the various parameters of the first example used in Sec. V, i.e.,

$$\frac{\bar{P}_r}{N_0} = 29 \text{ db}$$

$$B = 7 \text{ kcps}$$

$$L = 4 \text{ msec}$$

$$P_e = 10^{-5}$$

$$M = 2$$

The trial data rate divided by  $\log_2 M$  is marked on the abscissa of the upper left graph. This value of  $R/\log_2 M$  together with the curve corresponding to the value of  $\bar{P}_r/N_0 = 29$  db provides us with the actual value of

$$\frac{\bar{E}_s}{N_o} = \frac{\bar{P}_r}{N_o} \left( \frac{\log_2 M}{R} \right)$$

along the ordinate (Step 2). The value of  $R/\log_2 M$  together with the curve corresponding to the desired duty cycle ( $R/\log_2 M$ ) ( $1/T$ ) in the lower-left graph then gives the value of  $T$  along the ordinate of this graph (Step 3). This value of  $T$  together with the curve corresponding to the value of  $B = 7$  kcps in the lower-right graph provides us with the diversity  $n_d$  along the abscissa of this graph (Step 4). We now have a value of  $n_d$  as abscissa and a value of  $\bar{E}_s/N_o$  as ordinate for the upper-right graph and we may check these values to see if they are consistent with the curve corresponding to the desired error rate (Steps 5 and 6). A trial design is illustrated by dashed lines in Fig. 30 in which  $R$  was taken to be 10 bits/sec with a required duty cycle of 10 and the resulting value of required  $\bar{E}_s/N_o$  was greater than  $(\bar{P}_r/N_o) T_m$ , i.e., the design failed. A trial data rate of 7.5 bits/sec results in a satisfactory signal design for a duty cycle of 10.

A more complete set of design curves is given in Fig. 31. The upper-right graph is exactly Fig. 29 with abscissa  $n_d$  and ordinate  $\bar{E}_s/N_o = (\bar{E}_b/N_o) \log_2 M$  and the various curves correspond to different values of  $P_e/(M-1)$ . The lower-right curve shares its abscissa ( $n_d$ ) with the upper graph and the curves are plots of  $n_d = (T+L)/(1/T+B)$  vs  $T$  for  $L = 4$  msec (to correspond to the  $2r_e$  equatorial belt) and various Doppler spreads  $B$ . These curves are only applicable to simple pulse signals in which  $TW \approx 1$ . The upper-left graph takes a trial value of  $R/\log_2 M$  along its abscissa and provides the corresponding value of  $\bar{E}_s/N_o$  by use of the curve corresponding to the proper value of  $\bar{P}_r/N_o$ . Use of these design curves permits rapid checking of trial designs so that, starting with  $\bar{P}_r/N_o$ ,  $B$ ,  $M$ ,  $DC$ , and  $P_e$ , it is easy to generate values of data rates for various duty cycles and alphabet sizes  $M$ .

## B. LINK CALCULATIONS

In order to get some appreciation of the capacity of a communication link using the  $2r_e$  dipole belt, we present in this section tables of data rates for various transmitting and receiving stations that are assumed to be in the equatorial plane. This assumption allows us to use our prior calculations of path gain and Doppler spread for symmetrical east-west, equatorial links.

To be conservative, the three-year belt dimensions are used in the calculations. We do not include the reduction in multipath spread from that given in Eq. (18) (for belt-limited conditions) for very large antennas operating under beam-limited conditions. Hence, we take  $L = 4.0$  msec for all of the following computations. This is of no real consequence if optimum diversity can be achieved, which only occurs with large antennas. The transmitting and receiving station parameters are listed as follows.

<u>Transmitter</u>	<u>Receiver</u>
$D_t$ = antenna diameter (feet)	$D_r$ = antenna diameter (feet)
$P_{avg}$ = average transmitter power (watts)	$T_r$ = receiving system noise temperature ( $^{\circ}K$ )
$P_{peak}$ = transmitter peak or pulse power (watts)	

From Table II we obtain values of  $\bar{P}_r/P_t$  for various antenna sizes. We then compute

$$\frac{\bar{P}_r}{N_o} = P_{avg} \cdot \frac{\bar{P}_r}{P_t} \cdot \frac{1}{kT_r}$$

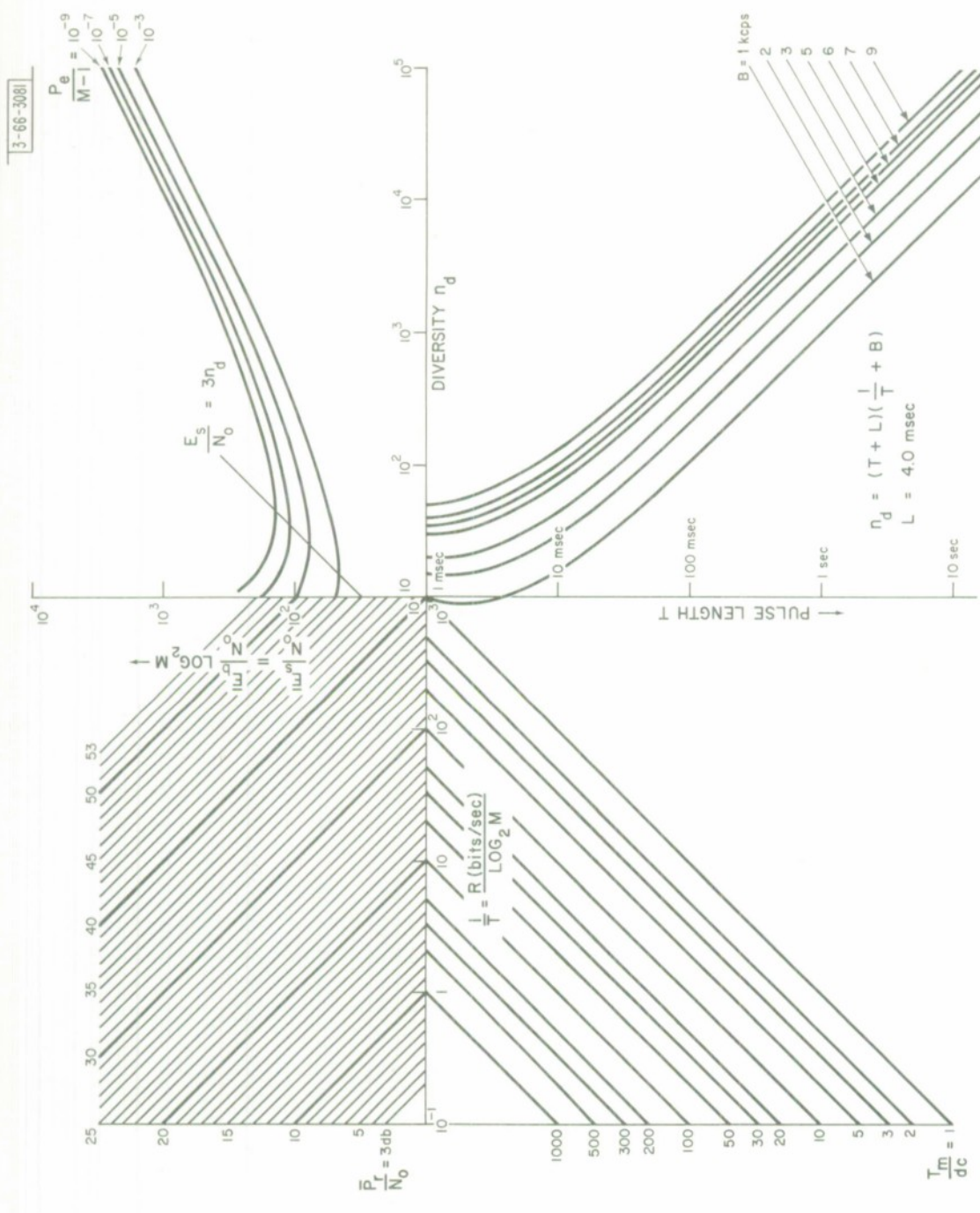


Fig. 31. Design curves for dipole belt channel.

where  $k$  is Boltzmann's constant. Multipath spread  $L$  is taken as 4.0 msec and Doppler spread  $B$  is given in Table III for various antenna sizes. The allowable duty cycle  $DC$  has been specified with the inclusion of  $P_{peak}$  as a transmitter parameter, and  $DC = P_{peak}/P_{avg}$ . All that remains is to decide on the required error rate  $P_e$  and the alphabet size  $M$ . We can then begin the graphical signal design procedure described in the previous section with the link parameters  $\bar{P}_r/N_o$ ,  $L$ ,  $B$ ,  $M$ , and  $P_e$ .

Tables IV and V present the results of graphical data rate computations for a wide variety of typical stations. The error rate has been taken as  $10^{-5}$  throughout the computation. Binary systems are included in Table IV, and Table V treats systems in which  $M = 32$ . Two data rates are given for each link, the upper one being the maximum rate consistent with the transmitter peak power requirement and the lower rate corresponding to CW operation of the transmitter. The maximum rate sometimes corresponds to pulse operation with duty cycle  $dc \leq DC$  (usually in small stations) and sometimes to CW transmitter operation, in which data rates are high enough to allow such operation with optimum diversity (only very large stations).

TABLE IV BINARY SYSTEMS								
RECEIVER		Antenna Diameter (feet) Noise Temperature (°K)	TRANSMITTER					Antenna Diameter (feet) Transmitter Average Power (kw) Peak Power (kw)
			2	6	15	30	60	
			10	10	20	25	100	
		50	50	100	100	100		
RECEIVER	2	200	/	/	/	<0.1 / <0.1	0.7 / 0.7	
	6	200	/	<0.1 / <0.1	<0.1 / <0.1	1.5 / 0.45	20 / 20	
	15	100	/	<0.1 / <0.1	2.0 / 0.45	18 / 0.45	150 / 150	
	30	100	<0.1 / <0.1	0.35 / <0.1	5.5 / 1.8	40 / 25	350 / 350	
	60	75	0.20 / <0.1	2.0 / 0.45	20.0 / 9.0	110 / 100	1000* / 1000*	

- (1) Two data rates (bits/sec) are given in each box. The upper one corresponds to pulse operation of the transmitter consistent with its peak power limitation. The lower rate corresponds to CW transmitter operation.
- (2) The data rate calculations are based on an error rate of  $10^{-5}$ .
- (3) A 5-db margin has been included in the data rate calculations.
- (4) The particular link geometry assumed is the 13,000-km equatorial link described in Sec. IV. The calculations are conservative in that they assume three-year belt dimensions.
- (5) The asterisk denotes the cases in which the maximum data rate is achieved with optimum diversity.

(These notes apply also to Table V.)

TABLE V  
M-ARY SYSTEMS

		TRANSMITTER					Antenna Diameter (feet) Transmitter Average Power (kw) Peak Power (kw)
		2	6	15	30	60	
RECEIVER	Antenna Diameter (feet) Noise Temperature (°K)	2	6	15	30	60	
		10	10	20	25	100	
		50	50	100	100	100	
	2 200	/	/	/	<0.5/ / <0.5	2.5/ / 2.5	
	6 200	/	<0.5/ / <0.5	<0.5/ / <0.5	6.0/ / 1.7	75/ / 75	
	15 100	/	<0.5/ / <0.5	9.0/ / 1.7	70/ / 35	650/ / 650	
	30 100	<0.5/ / <0.5	1.25/ / <0.5	20/ / 7.0	150/ / 110	1300* / 1300*	
	60 75	0.60/ / <0.5	9.0/ / 1.7	75/ / 35	450/ / 375	3800* / 3800*	

## VII. EPILOGUE

### A. SUMMARY

In an effort to understand some of the problems involved in dipole belt system design, we have considered in detail the design of a belt with potential use in government communication systems. This belt typifies a minimal-cost belt system that can meet many military requirements. It consists of 800 kg of dipoles in an equatorial belt at an altitude of two earth radii above the earth, and permits long links (up to 13,000 km) between sites in all parts of the world except around the poles. About 87 percent of the earth's surface can be served by such a belt. The data rates available via the  $2r_e$  belt are modest, but should be satisfactory for many military needs. Between two small terminals (15-foot antennas) separated by 13,000 km, a rate of up to 9 bits/sec can be attained with a signalling scheme that provides good station-to-station interference resistance; from a 15-foot antenna terminal to a 60-foot terminal at the same distance, a rate of 75 bits/sec can be obtained for conditions described in Sec. VI. This dipole belt has an indefinite orbital lifetime. In the course of describing the  $2r_e$  belt, we have touched on many elements of dipole belt design techniques. It is now time to emphasize those aspects of belt system design left unexplored, and to review some of the items which require investigation before even the  $2r_e$  belt system could be implemented.

### B. APPLICABILITY OF THIS REPORT

The mechanical properties of a dipole belt present a major problem to a belt system designer, whereas the electrical properties do not. For example, prediction of belt behavior requires computer simulation of many individual dipoles, each subject to the random effects of dispensing and micrometeoroid impacts. Slight changes in the launch conditions, dispensing technique, or in environmental assumptions often produce striking differences in belt behavior. Gross belt behavior, such as bounds on belt life or variation of belt orbital elements with time can sometimes be inferred from the launch conditions without extensive simulation. Nonetheless, in choosing one or more belts to implement a communication system, some simulation will need to be done. Unfortunately, no procedure has been found that will systematize and simplify the designer's task; that is, for a given set of design requirements, no technique is known for a general search procedure by which one finds the belt system parameters which specify a system having the desired characteristics. In fact, one cannot tell whether or not a system meeting the requirements exists. For each prospective design, one must therefore attempt to enumerate typical examples of feasible designs. A comparison among the examples will then, hopefully, lead to a satisfactory choice.

Because a dipole belt's size and shape is quite sensitive to parameters describing its initial launch conditions, and because a wide variety of belts is possible, a general treatment of belt coverage is lengthy. This report, for the sake of clarity, considered coverage only for the  $2r_e$  belt system. Part of this treatment, especially that on visibility computations, is general, but much of it is not. For instance, the coverage computation for nonequatorial belts must take into account the earth's rotation. When systems of belts are examined, the relative locations of the belts must be chosen to give maximum coverage. These modifications add significantly to the complexity of the coverage calculations, but can be systematically handled. Another variation, which does not involve much additional computation, uses a different

coverage criterion. In this report, for example, we insisted on continuous (24-hour/day) coverage, whereas an average coverage measure, as is more commonly used in the design of active repeater satellite systems, could have been used.

A more comforting note is provided by the results on dipole belts as communication channels and on the signal design for such a channel. All dipole belts are well characterized by the simple channel model adopted in this work, and many of the computations of the model parameters in Sec. IV can be used for other dipole belts. In general, belt cross-section major and minor axes are not always so conveniently aligned with the in-plane and out-of-plane directions as is the case with the  $2r_e$  belt, but the alignment can be readily taken into account. The signal design procedure applies to any dipole belt, and, in fact, the type of signalling technique of Sec. V can apply not only to dipole belts, but also to a channel using the moon or an active repeater satellite.

### C. CAVEAT EMPTOR

Several assumptions made in arriving at the  $2r_e$  belt system were based on estimates which require verification. These are:

- (1) Feasibility of dispenser design,
- (2) Effect of dipole coating,
- (3) Effect of dipole production techniques on orbital behavior.

The dispenser assumed for the  $2r_e$  belt uses dipoles aligned along the circumference of the dispenser spin axis, whereas the West Ford dispenser had dipoles aligned along the spin axis. Thus, the dispensing system required for the  $2r_e$  belt needs to be designed, and must accommodate about 800 kg of copper dipoles. The proper dispensing of dipoles from such a dispenser must then be verified to ensure that the circumferential wrapping does not have undesired effects on the dipole release mechanism. In addition, it is appropriate to study the effects of the production techniques necessitated by this dispenser on the dipole behavior in orbit. For instance, the reflectivity of the ends of the dipoles may modify the effects of solar radiation pressure on the dipole orbits. The effectiveness of the dipole blackening in reducing reflectivity needs further measurement, and tests need to be conducted on the longevity of the blackening in a space environment. Also, one should not exclude from consideration reflector shapes other than the straight or slightly curved dipole. Materials other than copper may provide useful features (such as disposability) which merit examination.

In addition to these unresolved questions, the validity of the simulation program parameters must always be considered. Any new information concerning parameters, such as experimental observation of meteoroid rates or of the solar radiation pressure constant, may have some effect on the results of the simulation.

One last unresolved feature of the  $2r_e$  belt system relates to the system organization and operational plan. Any actual communication system design must give detailed attention to the network organization, and must especially consider the means by which the network can be reorganized as station location and functions change.

APPENDIX A  
UPPER BOUND ON BINARY ERROR PROBABILITY

We will first derive an exponential upper bound on probability of error applicable to any binary communication system in which two separate receivers perturbed by independent additive noises may be used to detect each of the possible transmitted signals. The receiver then decides which signal was transmitted on the basis of the larger of the two receiver outputs. We will then specialize this bound to the simplified channel model of a dipole belt channel developed in Sec. V.

We will adopt the notation in Sec. V in which  $p_s(y)$  and  $p_n(y)$  were taken to be the probability densities of the outputs of the receiver operating on signal plus noise and the receiver operating on noise alone, respectively [Eqs. (35) and (38)]. The probability of error may then be written as

$$P_e = \int_{-\infty}^{\infty} \left[ \int_{-\infty}^y p_s(\xi) d\xi \right] p_n(y) dy \quad (A-1)$$

The inner integral may be written as

$$\int_{-\infty}^y p_s(\xi) d\xi = \int_{-\infty}^{\infty} p_s(\xi) \mu(\xi) d\xi \quad (A-2)$$

where we have defined the function

$$\mu(\xi) = \begin{cases} 1 & \text{for } \xi \leq y \\ 0 & \text{for } \xi > y \end{cases}$$

From Fig. A-1 it is easy to see that

$$\mu(\xi) \leq e^{s(\xi-y)}, \quad s \leq 0 \quad (A-3)$$

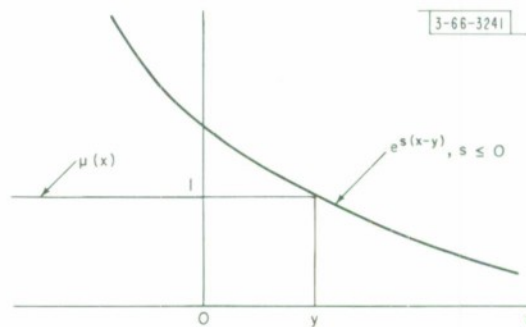
so that Eq. (A-2) becomes

$$\begin{aligned} \int_{-\infty}^y p_s(\xi) d\xi &\leq e^{-sy} \int_{-\infty}^{\infty} p_s(\xi) e^{s\xi} d\xi \\ &= e^{-sy} g_s(s), \quad s \leq 0 \end{aligned} \quad (A-4)$$

and  $g_s(s)$  is the moment generating function of the output of the receiver operating on signal plus noise. Thus we arrive at the bound on error probability as

$$P_e \leq g_s(s) \int_{-\infty}^{\infty} e^{-sy} p_n(y) dy = g_s(s) g_n(-s), \quad s \leq 0 \quad (A-5)$$

Fig. A-1. Upper bound on  $\mu(x)$ .



where  $g_n(s)$  is the moment generating function (MGF) of the output of the receiver operating on noise alone. This bound is most useful in cases where each of the receiver outputs is actually a sum of  $N$  independent random variables since in this case  $g_S(s)$  and  $g_n(s)$  can be written as products of the MGF's of the  $N$  random variables; that is

$$G_S(s) = g_S^N(s) \quad , \quad G_n(s) = g_n^N(s)$$

and

$$P_e \leq [g_S(s) g_n(-s)]^N \quad , \quad s \leq 0 \quad .$$

The bound is thus seen to have an exponential dependence on  $N$ .

At this point we can apply this bound to our dipole belt channel model in which each receiver output may be taken to be the sum of outputs corresponding to  $n_d$  independent degrees of diversity. The probability densities for the two receiver outputs for a single degree of diversity can be found from Eqs. (35) and (38) and are

$$p_S(y) = \frac{\exp\left[-\frac{y}{2a_S}\right]}{2a_S} \quad , \quad y \geq 0 \quad , \quad a_S > 0 \quad (A-6a)$$

$$p_n(y) = \frac{\exp\left[-\frac{y}{2a_n}\right]}{2a_n} \quad , \quad y \geq 0 \quad , \quad a_n > 0 \quad . \quad (A-6b)$$

It is easy to verify that for  $n_d = 1$  the desired moment generating functions are given by

$$g_S(s) = \int_0^\infty p_S(y) e^{sy} dy = \frac{1}{1 - 2a_S s} \quad , \quad s < \frac{1}{2a_S} \quad (A-7a)$$

$$g_n(s) = \int_0^\infty p_n(y) e^{sy} dy = \frac{1}{1 - 2a_n s} \quad , \quad s < \frac{1}{2a_n} \quad . \quad (A-7b)$$

The moment generating function of the receiver outputs for  $n_d$  independent degrees of diversity are thus

$$g_n^{(n_d)}(s) = (1 - 2a_S s)^{-n_d} \quad , \quad s < \frac{1}{2a_S} \quad (A-8a)$$

$$g_n^{(n_d)}(s) = (1 - 2a_n s)^{-n_d} \quad , \quad s < \frac{1}{2a_n} \quad . \quad (A-8b)$$

Note that  $g_n^{(n_d)}(-s)$  is defined for  $-s < 1/2a_n$  or  $-1/2a_n < s$ . Since the bound given by Eq. (A-5) requires that  $s \leq 0$ , we can write

$$P_e \leq [(1 - 2a_S s)(1 + 2a_n s)]^{-n_d} \quad , \quad -\frac{1}{2a_n} < s \leq 0 \quad . \quad (A-9)$$

The upper bound on  $P_e$  for a binary system with diversity  $n_d$  given above is a valid upper bound for any value of  $s$  in the acceptable range. We must now choose that value of  $s$  which

gives the best upper bound to  $P_e$ , that is, gives the minimum upper bound. Since the right-hand side of Eq. (A-9) is convex downward we know that any stationary point with respect to  $s$  is a minimum of the bound, but we must also have  $s$  in the interval  $(-1/2a_n) < s \leq 0$ . Differentiating the right-hand side of Eq. (A-9) and setting it equal to zero gives

$$-n_d [(1 - 2a_s s) (1 + 2a_n s)]^{-n_d} \left( \frac{2a_n}{1 + 2a_n s} - \frac{2a_s}{1 - 2a_s s} \right) = 0 \quad (A-10)$$

Since the left bracket is just our upper bound on  $P_e$  it cannot be zero in general, hence the right-hand bracket must be zero. The optimum value of  $s$ , called  $s_o$ , satisfies

$$\frac{2a_n}{1 + 2a_n s_o} = \frac{2a_s}{1 - 2a_s s_o}$$

and so

$$s_o = \frac{a_s - a_n}{4a_n a_s} \quad (A-11)$$

Now comparing Eqs. (A-6a and b) to Eqs. (35) and (38); we see that

$$\begin{aligned} a_n &= \sigma_n^2 > 0 \\ a_s &= \sigma_{s+n}^2 = \sigma_s^2 + \sigma_n^2, \quad \sigma_s^2 \geq 0 \end{aligned} \quad (A-12)$$

and so

$$a_s - a_n \geq 0 \quad (A-13)$$

Therefore, we can write  $s_o$  as

$$s_o = -\frac{1}{2a_n} \left( \frac{a_s - a_n}{2a_s} \right) = -\frac{1}{2a_n} \alpha, \quad 0 \leq \alpha < 1 \quad (A-14)$$

Combining Eqs. (A-13) and (A-14) then, we see that the optimum value of  $s$  satisfies

$$-\frac{1}{2a_n} < s_o \leq 0 \quad (A-15)$$

and is thus an acceptable value of  $s$ .

Finally, evaluating our upper bound at  $s = s_o$  results in

$$\begin{aligned} P_e &\leq \left[ \left( 1 + \frac{a_s - a_n}{2a_n} \right) \left( 1 - \frac{a_s - a_n}{2a_s} \right) \right]^{-n_d} \\ &= \left( \frac{a_n + a_s}{2a_n} \cdot \frac{a_s + a_n}{2a_s} \right)^{-n_d} \\ &= \left[ \frac{\left( 1 + \frac{a_s}{a_n} \right)^2}{4 \frac{a_s}{a_n}} \right]^{-n_d} \end{aligned} \quad (A-16)$$

We observe from Eqs. (A-12), (39), and (42)

$$\frac{a_s}{a_n} = 1 + \frac{\sigma_s^2}{\sigma_n^2} = 1 + \frac{\bar{E}_s}{n_d N_0} = 1 + a \quad (\text{A-17})$$

where  $a$  has been defined in Sec. V as the signal-to-noise ratio per degree of diversity. Thus

$$P_e \leq \left[ \frac{(2+a)^2}{4(1+a)} \right]^{-n_d} = \exp \left\{ -n_d \ln \left[ \frac{(2+a)^2}{4(1+a)} \right] \right\} = \exp \left[ -\frac{\bar{E}_s}{N_0} L(a) \right] \quad (\text{A-18a})$$

where

$$L(a) = \frac{1}{a} \ln \frac{(2+a)^2}{4(1+a)} \quad (\text{A-18b})$$

APPENDIX B  
2r<sub>e</sub> BELT PARAMETERS

The various parameters chosen for the 2r<sub>e</sub> belt are summarized in this Appendix.

I. DIPOLES

Length <sup>†</sup> (ℓ)	1.75 cm (0.689 inch)
Diameter (d)	0.00178 cm
Volume	4.4 × 10 <sup>-6</sup> cm <sup>3</sup>
Area <sup>‡</sup>	3.1 × 10 <sup>-3</sup> cm <sup>2</sup>
Copper density	8.9 gm/cm <sup>3</sup>
Mass	39.2 μgm
Area/mass	80.0 cm <sup>2</sup> /gm
Number of dipoles in payload of 1000 kg <sup>§</sup>	2 × 10 <sup>10</sup>
Optical reflectivity (specular)	5 percent

II. DISPENSER

Outer radius of dipole pack	45.7 cm (18 inches)
Inner radius of dipole pack	30.0 cm (11.8 inches)
Initial dispenser spin rate	2.69 rps (160 rpm)
Maximum tangential velocity	7.73 meters/ sec
Spin axis initially perpendicular to orbit plane	

III. ORBIT

Mean altitude (above earth)	2r <sub>e</sub>
Semi-major axis	3r <sub>e</sub>
Orbital period	7.3 hours
Orbital velocity (circular)	4.56 km/sec
Initial argument of perigee	0°
Initial longitude of ascending node	0°
Launch date	21 March 1965
Initial inclination <sup>¶</sup>	1°
Initial eccentricity	various values less than 0.06
Solar radiation pressure	46.5 × 10 <sup>-6</sup> dyne/cm <sup>2</sup>

<sup>†</sup> A dipole of this length is resonant of a frequency of 8 Gcps.

<sup>‡</sup> Maximum projected area ℓ × d.

<sup>§</sup> 20 percent of the payload is devoted to the dispenser.

<sup>¶</sup> A nonzero initial inclination is used to avoid a computational nuisance associated with a zero value. The inclination obtained in the simulation varies between 0.3° and 1.0°.

#### IV. MICROMETEOROID COLLISION MODELS

Given that a dipole-micrometeoroid collision has occurred, the probability that the dipole gains linear momentum exceeding  $p$  in magnitude is given by

$$P(\text{momentum} > p) = \begin{cases} \left[ \frac{p_{\min}}{p} \right]^k & , \quad p \geq p_{\min} \\ 1 & , \quad p < p_{\min} \end{cases}$$

where

$$p_{\min} = 7.75 \times 10^{-6} \text{ gm-cm/sec,}$$

$k = 1.7$ , and a dipole is assumed to have been severed if

$$p \geq 0.1 \text{ gm-cm/sec.}$$

Collision model A assumes a dipole-micrometeoroid collision rate of 5 per day; model B assumes one of 0.5 per day. The relationship of these two models to data derived from impact rate measurements<sup>7</sup> is shown in Fig. B-1.

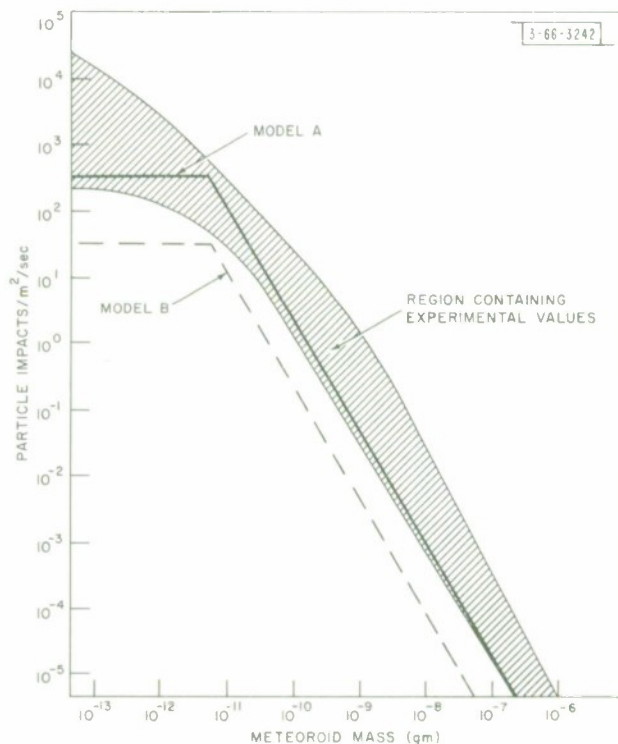


Fig. B-1. Comparison of simulation micrometeoroid models with experimental values.

APPENDIX C  
ORBITING DIPOLES AS PUNCTURE HAZARD

An estimate of the hazard presented by a dipole belt in orbit to satellites passing through the belt is given in this Appendix. This estimate is based on hypervelocity impact experiments performed at the NASA Ames Research Center.

I. COLLISION RATE

The determination of the probability of collisions between a satellite passing through a dipole belt and dipoles within it requires several parameters:

- $\vec{v}_d$  dipole velocity
- $\vec{v}_s$  satellite velocity
- $\rho$  dipole density
- L dipole belt width along  $\vec{i}_\ell$ , a unit vector perpendicular to  $\vec{v}_d$  and in the plane of  $\vec{v}_d$  and  $\vec{v}_s$ .

From Fig. C-1, which is in the plane containing  $\vec{v}_d$  and  $\vec{v}_s$ , we see that the satellite remains in the belt for a time  $L/(\vec{v}_s \cdot \vec{i}_\ell)$ . Thus the effective belt volume swept out by a satellite presenting a square meter of intercept area along  $\vec{v} = \vec{v}_s - \vec{v}_d$  is  $L v/(\vec{v}_s \cdot \vec{i}_\ell)$ , where  $v = |\vec{v}|$ . Multiplying by the dipole density gives

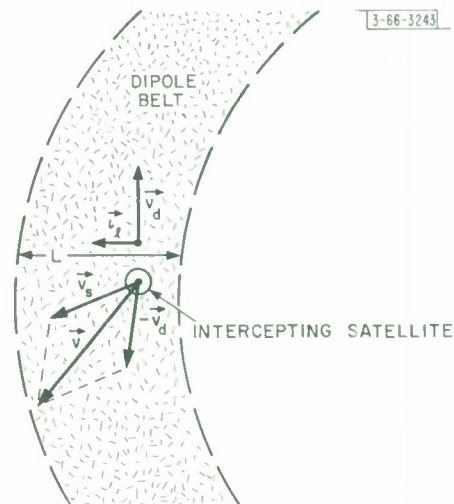
$$n = \frac{\rho L |\vec{v}_s - \vec{v}_d|}{\vec{v}_s \cdot \vec{i}_\ell} \tag{C-1}$$

as the average number of dipoles that is intercepted by a one-square-meter satellite during a single pass through the belt. If  $\vec{v}_s \cdot \vec{i}_\ell$  is zero, then  $\vec{v}_s$  and  $\vec{v}_d$  must be collinear, so the satellite is in the same orbit as the dipoles or in a counter-rotating orbit. In either case, the satellite remains in the belt indefinitely, which gives

$$n' = \rho vt \tag{C-2}$$

as the average number of dipoles intercepted by the satellite during time t.

Fig. C-1. Dipole-satellite collision geometry



As shown in Sec. II, the linear density of dipoles along the orbit is nearly uniform after a few months of belt life. For the  $2 \times 10^{10}$  dipoles of the  $2r_e$  belt† this means that the linear density of dipoles is about 16,700 dipoles/km. The volume density of dipoles  $\rho$  can then be obtained from the linear density by dividing by the belt cross-section area. The minimum value of the cross-section area should be used in order to maximize  $\rho$  and thus give a conservative estimate of the collision hazard. From Fig. 2, we see that within two months after dispensing, the cross-section area exceeds  $100 \text{ km}^2$  for the two simulated belts which use a nonzero collision rate model. Before the end of the first year, the minimum value has passed  $1000 \text{ km}^2$ . The  $100\text{-km}^2$  value will be used in this Appendix, and we get  $\rho = 167 \text{ dipoles/km}^3$ . Any other choice for the area will give a value for the collision hazard that varies inversely with the area; for example, an assumed area of  $1000 \text{ km}^2$  would give one-tenth the collision hazard obtained below.

Three cases of satellites intersecting the  $2r_e$  belt will be examined:

Counter-Rotating:- This satellite traverses the same orbit as the dipoles, but in the opposite direction. This extreme case cannot be maintained by a nonthrusting satellite because orbital perturbations will cause the satellite and belt orbits to separate.

Polar Orbit:- This satellite is in a roughly circular polar orbit of the same altitude ( $2r_e$ ) as the dipole belt, and intersects the belt twice each orbit.

Eseape:- This example is assumed to travel at escape velocity and passes radially through the belt at its maximum dimension. This represents the worst-case encounter for a translunar or other deep space vehicle.

For these three cases we obtain the following values for the expected collision rate with a one-square-meter target:

Trajectory	$v(\text{km/sec})$	$\vec{v}_s \cdot \vec{t}_\ell (\text{km/sec})$	Collisions per Square Meter in One		
			Orbit	Month	Year
Counter-rotating	9.12	0	40	4000	48,000
Polar orbit	6.34	4.56	$7.0 \times 10^{-3}$	0.70	8.4
Eseape	11.9	11.0	$9 \times 10^{-3}$	-	-

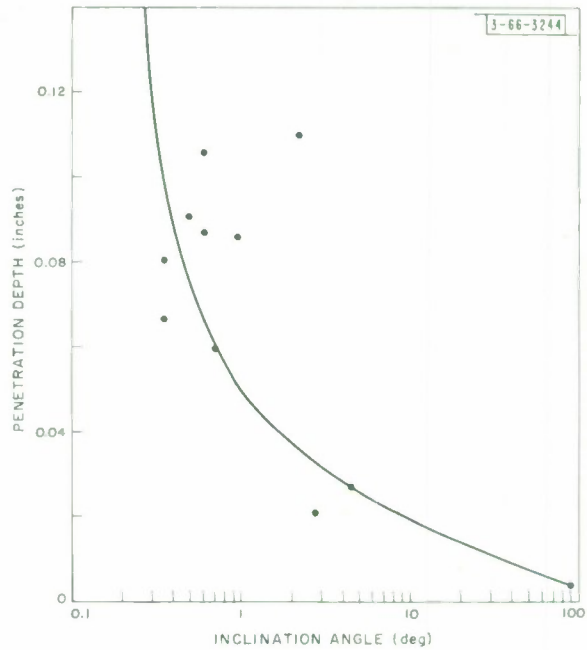
In this tabulation, a value of 500 meters was used for  $L$  for the escape trajectory, and 30 meters for the polar orbit case, as obtained from Fig. 1 by using the maximum values of in-plane and out-of-plane spread, respectively.

## II. COLLISION DAMAGE

Experimental determination of the penetration depth of thin copper rods into metallic targets under hypervelocity impact has been made by several authors.<sup>23-26</sup> Most of these tests were conducted at velocities considerably less than would occur in satellite-dipole collisions, and used rods of larger cross section than the dipoles discussed in this report. Some recent experiments conducted at the NASA Ames Research Center by C. R. Nysmith<sup>9</sup> are the most useful for the

† See Appendix B for belt parameters.

Fig. C-2. Copper filament-aluminum sphere impact data.



collision hazard computation because the copper filaments used were 0.7 inch in length and 0.0007 inch in diameter, the same dimensions as assumed for the dipoles in this report. The test firings were conducted at velocities of about 4 km/sec and made use of the same procedure as an earlier test with 0.0025-inch filaments.<sup>26</sup> The results from these tests are reproduced in Fig. C-2, corrected to 15,000 ft/sec (about 4.5 km/sec). Precise measurements of the inclination angle (the angle between the filament axis and the collision velocity vector) were difficult to make because of some uncertainty in the position of the filament at the time of impact and because the filaments may not have been entirely straight. Nysmith has provided the following observations based on test firings:

- (a) The maximum penetration expected from perfectly end-on impacts of straight filaments at 15,000 ft/sec is about 0.7 inch, the length of the filament.
- (b) The  $3/2$  scaling law generally adopted for converting the penetration thickness of very thick targets into the perforation thickness of thin targets does not seem to apply to filament collisions, except, perhaps for broadside impact.
- (c) Substantial filament curvature seems to make the impact depth independent of the filament inclination. For filaments of 0.0029-inch diameter, 0.7 inch long, and with radii of curvature of from 1 to 3 inches, a penetration depth of 0.25 inch was obtained for many different orientations. This may be compared with tests of straight filaments for which penetrations of 0.013 to 0.45 inch were encountered.

We now proceed with the hazard probability calculation. If dipole orientations are uniformly distributed among all possible orientations,<sup>†</sup> the probability that a dipole is inclined by an angle

<sup>†</sup> The dipole orientation is regarded as fixed for the duration of the impact because its maximum change is limited to  $0.05^\circ$  under the condition of maximum spin rate and longest possible collision time.

$\theta \leq \alpha$  relative to a given axis is equal to the probability that its axis lies within a cone about that axis with apex angle  $\alpha$ . This is given, in turn, by the ratio of the sphere surface area intercepted by such a cone to half the sphere's surface area, or

$$p(\theta \leq \alpha) = \frac{2\pi \int_0^\alpha \sin x \, dx}{2\pi} = 1 - \cos \alpha \quad (C-3)$$

Combining the experimental values from Fig. C-2 with Eq. (C-3) gives the curve of Fig. C-3 for the conditional probability of penetration in excess of a certain depth, given that a dipole collision has occurred, with collisions into aluminum targets at velocities of 4.5 km/sec. The probability of penetration of an aluminum target in the orbits described earlier can now be made. The target is here assumed to have a 1/8-inch-thick aluminum skin, and to present one square meter of target area. The results are shown below.

Trajectory	Penetration Probability
Counter-rotating	0.24 for one month in the belt
Polar orbit	$3.5 \times 10^{-4}$ for one year in the belt
Escape	$7.1 \times 10^{-9}$ for each pass

The results of Fig. C-3 were scaled linearly with velocity in computing this table.

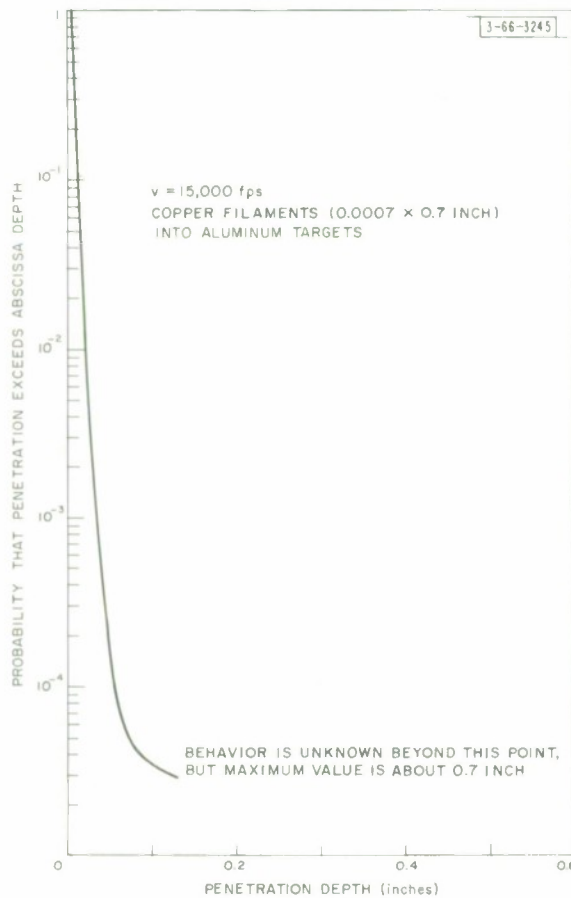


Fig. C-3. Dipole penetration probability.

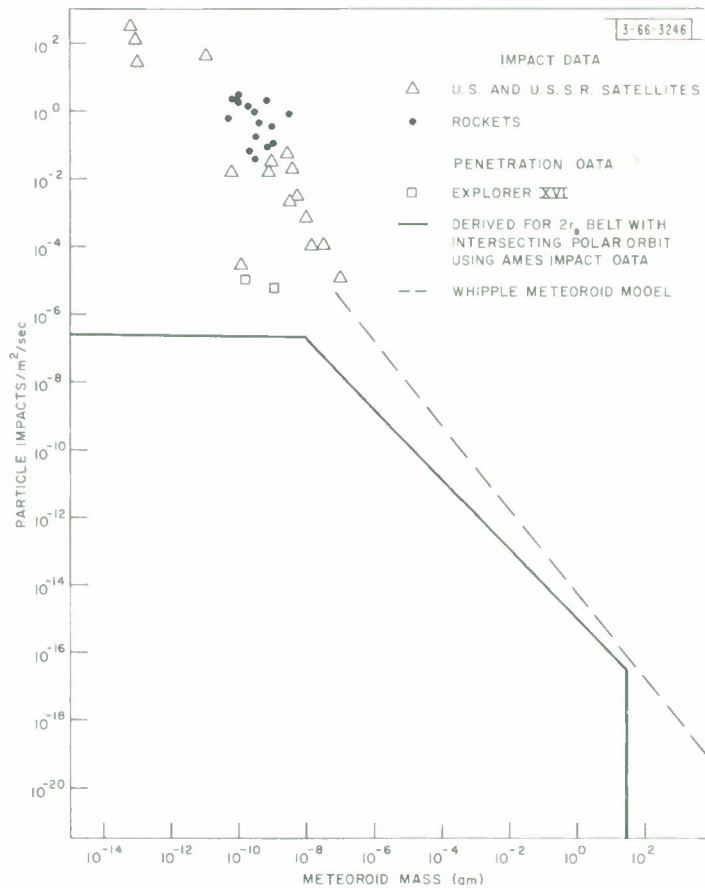


Fig. C-4. Comparison of the dipole hazard with the natural meteoroid background.

A comparison of the hazard presented by a dipole belt with that which exists naturally in the micrometeoroid environment can be made on the basis of the experimental impact information described above and that obtained from artificial satellites. Figure C-4 shows the micrometeoroid influx rate according to particle size as obtained from various direct measurements,<sup>7,27</sup> from a recent calculation of Whipple based on photographic meteor studies<sup>10</sup> and from the penetration depth curve on the basis of a polar orbit intersecting the  $2r_c$  belt. This last calculation is obtained from Fig. C-3 and Eq. (C-1), with the assumption that meteoroids with a mean density of  $0.44 \text{ gm/cm}^2$  and a mean velocity of  $30 \text{ km/sec}$  (as in Ref. 10) give rise to the penetration depths of Fig. C-3 using Bjork penetration criteria.<sup>27,28</sup>

## ACKNOWLEDGMENT

We wish to express thanks to Barney Reiffen for his many valuable suggestions, and for his patient reading of the many drafts of this report, and also to Herbert Sherman with whom this study originated. Thanks are also due to Harrison M. Jones for providing the dipole belt computer simulation program and to Maxine Check for writing many computer programs.

## REFERENCES

1. C. F. J. Overhage and W. H. Radford, "The Lincoln Laboratory West Ford Program - An Historical Perspective," *Proc. IEEE* 52, 452 (1964).
2. I. I. Shapiro, *et al.*, "Orbital Properties of the West Ford Dipole Belt," *Proc. IEEE* 52, 469 (1964).
3. *Aviation Week and Space Technology* 79, 221 (22 July 1963).
4. P. Waldron, *et al.*, "The West Ford Payload," *Proc. IEEE* 52, 571 (1964).
5. I. I. Shapiro, "The Prediction of Satellite Orbits," in *Dynamics of Satellites*, M. Roy, ed. (Academic Press, New York, 1963), pp. 257-312.
6. D. F. Edwards and M. C. Crocker, Lincoln Laboratory, M. I. T., private communication.
7. W. M. Alexander, *et al.*, "Review of Direct Measurements of Interplanetary Dust from Satellites and Probes," in *Space Research III*, W. Priester, ed. (North-Holland, Amsterdam, 1963), pp. 891-917.
8. W. Liller, "Optical Effects on the 1963 Project West Ford Experiment," *Science* 143, 437 (1964).
9. C. R. Nysmith, NASA Ames Research Center, private communication.
10. F. L. Whipple, "On Meteoroids and Penetration," in *Advances in the Astronautical Sciences* (American Astronautical Society, 1963), Vol. 13.
11. C. D. May, Jr., "The Significance of Military Communication Satellites," *Trans. IRE, PGMIL MIL-4*, 176 (1960).
12. F. E. Heart, *et al.*, "Measured Physical Characteristics of West Ford Belt," *Proc. IEEE* 52, 519 (1964) or I. L. Lebow, *et al.*, "The West Ford Belt as a Communications Medium," *Proc. IEEE* 52, 543 (1964).
13. B. Reiffen and M. H. Check, "Average Scattering Cross Section of Randomly-Oriented Dipoles," Group Report 65G-8, Lincoln Laboratory, M. I. T. (December 1963), DDC 427756, H-555.
14. C. L. Mack, Jr. and B. Reiffen, "RF Characteristics of Thin Dipoles," *Proc. IEEE* 52, 533 (1964).
15. R. P. Rafuse, "Characterization of Noise in Receiving Systems," in *Lectures on Communication System Theory*, E. J. Baghdady, ed. (McGraw-Hill, New York, 1961), Chap. 15.

16. A. S. Dennis and R. T. Callis, "Attenuation of SHF Signals by Precipitation at a Proposed Communication Satellite Terminal," Stanford Research Institute Research Memorandum 3 (February 1962).
17. G. N. Krassner and J. V. Michaels, Introduction to Space Communication Systems (McGraw-Hill, New York, 1964).
18. B. E. Nichols and D. Karp, "West Fard Radar and Microwave Equipment," *Prac. IEEE* 52, 576 (1964).
19. H. Cramer, Mathematical Methods of Statistics (Princeton University Press, Princeton, 1946), p. 233.
20. J. N. Pierce, "Theoretical Diversity Improvement in Frequency-Shift Keying," *Prac. IRE* 46, 933 (1958).
21. H. L. Yudkin, "An Error Bound for Gaussian Signals in Gaussian Noise," Quarterly Progress Report No. 73, Research Laboratory of Electronics, M. I. T. (15 April 1964).
22. R. S. Kennedy and I. L. Lebow, "Signal Design for Dispersive Channels," *IEEE Spectrum* 1, 231 (1964).
23. J. L. Summers and W. R. Niehaus, "A Preliminary Investigation of the Penetration of Slender Metal Rods in Thick Metal Targets," NASA Technical Note, NASA TN D-137 (December 1959).
24. R. E. Slattery and W. G. Clay, "The Penetration of Thin Rods into Aluminum" in "Hypervelocity Impact - Fourth Symposium, April 26-28, 1960," Air Proving Ground Center, APGC-TR-60-39 (111) (September 1960).
25. W. A. Allen, et al., "Penetration of a Rod into a Semi-Infinite Target," *J. Franklin Inst.* 272, 275 (1961).
26. C. R. Nysmith, et al., "Investigation of the Impact of Copper Filaments into Aluminum Targets at Velocities to 16,000 Feet per Second," NASA Technical Note, NASA TN D-1981 (February 1964).
27. C. T. D'Aiutala, "Review of Meteoroid Environment Based on Results from Explorer XIII and Explorer XVI Satellites," Space Research IV, P. Muller, ed. (North-Holland, Amsterdam, 1964), pp. 858-874.
28. R. L. Bjark, "Meteoroids vs Space Vehicles," *J. Am. Rocket Soc.* 31, 803 (1961).

## DOCUMENT CONTROL DATA - R&amp;D

(Security classification of title, body of abstract and indexing annotation must be entered when the overall report is classified)

1. ORIGINATING ACTIVITY (Corporate author) Lincoln Laboratory, M. I. T.		2a. REPORT SECURITY CLASSIFICATION Unclassified	
		2b. GROUP	
3. REPORT TITLE Study of an Orbiting Dipole Belt Communication System			
4. DESCRIPTIVE NOTES (Type of report and Inclusive dates) Technical Report			
5. AUTHOR(S) (Last name, first name, initial) Belvin, F.      Goblick, T. J., Jr.			
6. REPORT DATE 22 December 1964		7a. TOTAL NO. OF PAGES 86	7b. NO. OF REFS 28
8a. CONTRACT OR GRANT NO. AF 19 (628)-500		9a. ORIGINATOR'S REPORT NUMBER(S) Technical Report 369	
b. PROJECT NO.		9b. OTHER REPORT NO(S) (Any other numbers that may be assigned this report) ESD-TDR-64-591	
c.			
d.			
10. AVAILABILITY/LIMITATION NOTICES			
11. SUPPLEMENTARY NOTES		12. SPONSORING MILITARY ACTIVITY Air Force Systems Command, USAF	
13. ABSTRACT  The design of communication systems utilizing orbiting dipole belts is complicated by the great amount of interaction among the various design parameters involved. This interaction makes difficult a general treatment of the design problem for such systems, necessitating the study of specific examples. This report studies in detail the simplest example of such a system in which a single equatorial dipole belt is used. An altitude of 8000 miles is used to provide satisfactory earth coverage. This altitude precludes the possibility of a limited orbital lifetime belt. An 800-kg payload of X-band, copper dipoles would provide modest data rates which should suffice for certain military needs. Insofar as a specific belt configuration and dipole design were chosen, the specific results of this work do not apply to dipole belt systems in general. However, the considerations that receive attention, and the approach used in dealing with them, can be used as a guide in the design of any dipole belt communication system.			
14. KEY WORDS  satellite communication      communication systems      orbiting dipole belt passive communication satellites      multipath channels			